University of Wisconsin Milwaukee
UWM Digital Commons

May 2015

Microbially Induced Sedimentary Structures as an Ecological Niche in Subtidal Early Triassic Environments of Eastern Panthalassa

Erin Wimer
University of Wisconsin-Milwaukee

Follow this and additional works at: https://dc.uwm.edu/etd

Part of the Ecology and Evolutionary Biology Commons, Geology Commons, and the Paleontology Commons

MICROBIALLY INDUCED SEDIMENTARY STRUCTURES AS AN

ECOLOGICAL NICHE IN SUBTIDAL EARLY TRIASSIC ENVIRONMENTS

OF EASTERN PANTHALASSA

by

Erin E. Wagner

A Thesis Submitted in

Partial Fulfillment of the

Requirements for the Degree of

Master of Science

in Geosciences

at

The University of Wisconsin-Milwaukee

May 2015

ABSTRACT

MICROBIALLY INDUCED SEDIMENTARY STRUCTURES AS AN ECOLOGICAL NICHE IN
SUBTIDAL EARLY TRIASSIC ENVIRONMENTS OF EASTERN PANTHALASSA

by

Erin Wagner

The University of Wisconsin-Milwaukee, 2015
Under the Supervision Dr. Margaret Fraiser, PhD

Early Triassic microbially induced sedimentary structures (MISS) are a critical link in understanding the dynamics between changing environmental conditions and their effect on marine communities. The Permo-Triassic mass extinction (PTME) resulted in vacated ecospace and reduced bioturbation that allowed MISS to expand into Early Triassic subtidal environments. Data from southern Idaho and Montana indicate that MISS inhabited and proliferated in subtidal marine environments during the Griesbachian. This propagation led to changes in shallow substrate geochemical conditions that directly affected macrofaunal communities. The proliferation of microbial mats would have created anoxic and euxinic porewaters and made vertical bioturbation physiologically difficult. Geochemical data shows the bottom water signals associated with MISS were oxic to suboxic, but the porewaters below the microbial mat surface could have been anoxic even if the overlying water column was oxygenated. However, some metazoans adapted to these low-oxygen, shallow euxinic environments, allowing them to expand their ecological range during this period of crisis.   Two

metazoans with such adaptations were the lingulid brachiopods, which have the ability to oxidize hydrogen sulfide in their blood, and the bivalve *Claraia,* which was well suited to low oxygen environments. These specific disaster taxa, defined as opportunists that occupy vacated ecospaces during recovery periods but are subsequently forced into marginal settings when the recovery gains momentum, were found in direct contact with these MISS. These findings indicate that the subtidal proliferation of MISS during the Early Triassic provided an ecological niche in which specific metazoans had complex and extensive relationships.

iv

TABLE OF CONTENTS

LIST OF FIGURES

LIST OF TABLES

Chapter 1: Introduction

<u>Permo-Triassic Mass Extinction:</u>

During the Permo-Triassic mass extinction (PTME), the largest extinction in Earth's history, an estimated 49% of all marine families and 78% of all marine genera went extinct (e.g., Raup, 1979; Clapham et al., 2009). Recent U-Pb zircon dating of ash beds within the Global Stratotype Section and Point (GSSP) in Meishan, China has constrained the extinction between 251.941 ± 0.037 and 251.880 ± 0.031 Mya (Burgess et al., 2014). This interval of 60 ± 48 ka represents the main extinction event (Burgess et al., 2014).

Multiple causes have been proposed for the PTME. One of the largest triggers was likely the long term eruption of flood basalts from the Siberian Traps (e.g., Shen et al., 2012). It is hypothesized that the bulk of the eruptions occurred during an approximately one million year interval prior to 251.7 ± 0.4 Ma (Kamo et al, 2003; Black et al. 2012). $^{40}Ar/^{39}Ar$ isotope ages from the Noril'sk region in the western Siberian Basin, the Lower Tunguska area on the Siberian craton, the Taimyr Peninsula, the Kuznetsk Basin, and Vorkuta in the Polar Urals of Russia show that volcanic activity in Siberia covered up to 5 million km^2 (Reichow et al., 2009; Burgess et al., 2014). Based on the basaltic rock record in Siberia, these eruptions likely delivered massive pulses of volatiles into the atmosphere including sulfur, chlorine, and fluorine as well as carbon dioxide and methane (Retallack, 1999; Retallack & Jahren, 2008; Black et al, 2012). The estimated total magmatic degassing from these eruptions are: 6300 to 7800 Gt of sulfur, 3400 to 8700 Gt of chlorine, and 7100 to 13,600 Gt of fluorine (Black et al., 2012). The

injection of these volatiles into the upper atmosphere would have had effects ranging from toxicity, acid rain, temperature changes, ozone depletion and ocean acidification (Black et al., 2012).

While evidence for the duration and extent of the Siberian Trap eruptions in the late Permian is fairly well constrained, the environmental and ecological implications are not fully understood (Benton & Twitchett, 2003; Algeo et al., 2011; Shen et al., 2012). Evidence suggests the likely trigger for the dramatic climate change during the PTME was the release of volcanic carbon dioxide and methane (Retallack & Jahren, 2008; Algeo et al., 2011). Interconnected to the massive release of greenhouse gases were the episodic anoxic, sulfidic, and hypercapnic conditions in platform and continental margin settings seen at the peak of the end Permian and into the Early Triassic (Nielsen & Shen, 2004; Algeo et al., 2011). These conditions were primarily due to enhanced continental weathering and the gradual warming of the ocean (Nielsen & Shen, 2004; Algeo et al., 2011). Data suggest an ~10°C increase in ocean temperatures that immediately predated or postdated the extinction, which indicates an approximately 1°C rise in ocean temperature per 6,000 years of the extinction (Sun et al., 2012; Burgess et al., 2014). Evidence also indicates a sharp negative spike in the carbon isotope record that preceded the extinction event, with instability in the carbon cycle that continued for approximately 500ka (e.g., Burgess et al., 2014).

Increases in vanadium and molybdenum are seen in the rock record directly after the extinction event. Trace element concentrations are indicators of reducing conditions, with vanadium and molybdenum being particularly useful when determining

anoxia as they both preferentially concentrate in sediments of low oxygen (Calvert and Pederson 1993; Tribovillard et al., 2006). The first spike of vanadium does not coincide with any other trace element trends, suggesting mildly reducing conditions, and a first step reducing of vanadium (Calvert and Pederson, 1993; Kloss, 2012). Another spike coincides with a Mo increase, which indicates more strongly reducing conditions and the second step reducing of vanadium indicating both anoxic and euxinic conditions (Takahashi et al., 2014). Additionally, decreases in manganese and increases in chromium concentrations across the event horizon both indicate further reducing conditions (Takahashi et al., 2014).

Under normal, oxic conditions, $^{138}Ce/^{142}Ce$ ratios range from 0.2‰ to 0.6‰. At the P-T boundary, levels of $^{138}Ce/^{142}Ce$ increased to a range of 0.9‰ to 1.1‰, suggesting conditions were reducing (Takahashi et al., 2014). Similarly, Th/U ratios increased at the event horizon from 0.06 to 0.42, also indicating increasing anoxia across the extinction boundary (Brennecka et al., 2011). These ratios and concentrations can give a more detailed picture of the ocean chemistry changes that occurred, and how marine environments were directly affected at the event horizon and beyond. The presence of both significant anoxia and euxinia during the PTME were likely kill mechanisms for the extinction event.

Early Triassic Aftermath:

Evidence for Continued Environmental Stresses

Evidence for marine anoxia, euxinia, and hypercapnia (CO_2 poisoning), along with major shifts in the stable carbon isotope record is observed in the rock record well into the middle of the Triassic (e.g., Luo et al., 2011; Brennecka, 2011; Algeo et al., 2011). Continued stresses on Early Triassic biotic recovery were driven by significant changes in ocean chemistry as well as toxic atmospheric conditions that drove one another.

Significant attention has been paid to the negative $\delta^{13}C$ excursion that corresponds to the Permian-Triassic boundary, but excursions continued throughout the Early Triassic until stabilization was reached in the Middle Triassic (Payne et al., 2004; Rampino & Caldeira, 2005, Corsetti et al., 2005; Payne and Kump, 2007). Approximately 5my of Early Triassic $\delta^{13}C$ excursions reached values as high as +8‰ and as low as -3‰ in marine carbonates (Payne and Lehrmann, 2004; Payne and Kump, 2007).

Several causes for these negative excursions have been proposed, including instantaneous events like massive releases of methane or carbon dioxide, as well as protracted causes such as ocean stratification/turnover and the reorganization of the carbon cycle (e.g., Corsetti et al., 2005). Modeling by Payne and Kump (2007) has indicated that the negative $\delta^{13}C$ excursions resulted from carbon release with the isotopic signature of volcanic CO_2, and positive excursions are a result of increased pCO_2. They conclude that episodic thermal metamorphism of coal and carbonates during the eruption of the Siberian Traps is a likely explanation of the excursion fluctuations

throughout the Early Triassic and, once the volcanism subsided, the subsequent

recovery in the Middle Triassic occurred (Payne and Kump, 2007).
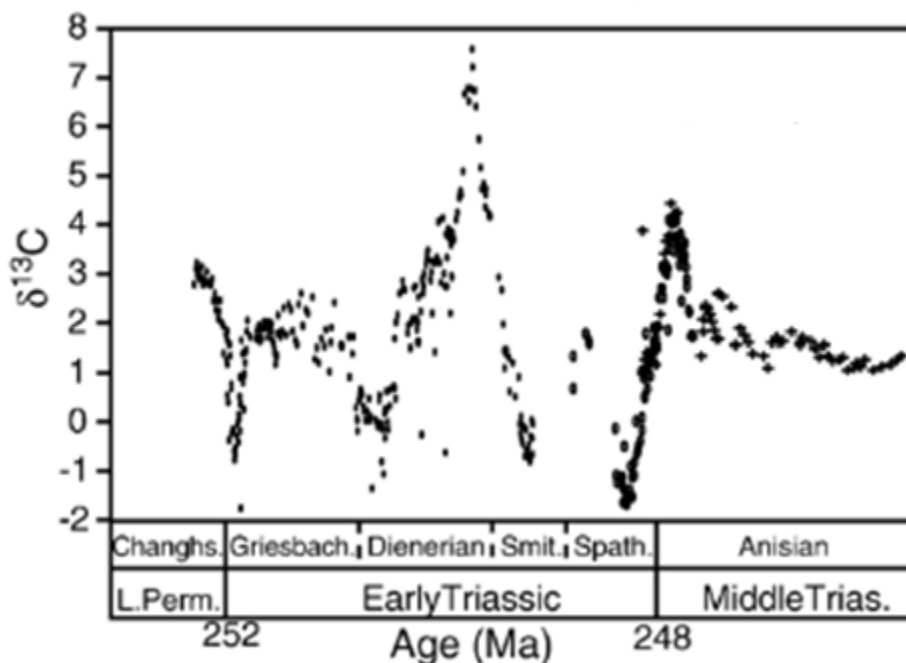
Figure 1. δ^{13}C record for the Late Permian through the Middle Triassic. δ^{13}C data from stratigraphic sections on the Great Bank of Guizhou in southern China. (Modified from Payne and Kump, 2007).

Euxinia during the Early Triassic is widely documented through the size and

abundance of ^{34}S-depleted pyrite framboids, as well as the sulfur isotopic record of

marine strata (Shen et al., 2007; Algeo at al., 2010, 2011). δ^{34}S records from shallow

marine sections indicate a negative excursion at the extinction horizon (-10 to -20‰)

and a positive shift (+20 to +40‰) in the approximately first million years of the Early

Triassic (Fig. 1) (Riccardi et al, 2006; Payne and Kump, 2007; Algeo et al., 2008). The

negative excursion at the Permian-Triassic Boundary (PTB) is likely due to an upwelling

of water from the deep ocean or a rising of the chemocline towards the surface, causing ^{34}S-depleted hydrogen sulfide to rise into the ocean surface waters (Kump et al., 2005; Algeo et al., 2008).

Previous studies on the Lower Triassic have suggested that bottom water anoxia and euxinia was widespread based on evidence from a limited geographical range of Panthalassan abyssal sections (Twitchett and Wignall, 1996; Algeo et al., 2011) However, recent geochemical evidence suggests localized anoxia and euxinia in an expanded oxygen minimum zone (OMZ), with suboxic conditions on Panthalassan bottom waters (Algeo et al., 2008, 2010, 2011). The abundance of pyrite framboids found in Early Triassic deep water sediments can be attributed to their formation higher in the water column (OMZ) and subsequent sinking to the seafloor (Algeo et al., 2008, 2010, 2011). Episodic upwelling of the OMZ waters would have brought anoxic and H$_2$S rich waters onto the shallow continental shelf and platforms (Algeo et al., 2010, 2011). Additionally, upwelling of carbon dioxide from the OMZ may have increased the acidity of the surface waters, the combination of which could have contributed to the protracted recovery during the Early Triassic (Fraiser and Bottjer, 2007, Algeo et al., 2011).

Evidence indicates that during the PTME a rapid climate change contributed to the extinction event in both marine and terrestrial ecosystems (Joachimski et al., 2012; Kiehl and Shields, 2014). This global climate shift was likely caused by the elevated atmospheric CO$_2$ levels following the eruptions of flood basalts from the Siberian Traps (Retallack & Jahren, 2008; Algeo et al., 2011) Global warming during the end Permian

into the Early Triassic would have resulted in shallow water anoxia due to poor ocean circulation and increased respiration of organic carbon (Wignall and Hallam, 1992; Knoll et al., 2007; Joachimski et al., 2012). Oxygen and carbon isotope data from in Bed 25 in Meishan, South China, and Bed 28a in Shangsi, South China both indicate an onset of poor oxygenated facies during the end Permian (Yan et al., 1989; Xie et al., 2007; Joachimski et al., 2012). These factors likely affected the protracted recovery of both marine and terrestrial ecosystems following the PTME (Knoll et al., 2007).

Biotic Recovery and Restructuring

It has been recently proposed that the aftermath from the PTME was protracted and lasted approximately 5 million years after the extinction event into the Middle Triassic (Lehrmann et al., 2006). While regional recovery and restructuring varied greatly, marine ecosystems generally showed the same trend of a rapid faunal decline during the PTME, minimal recovery during the Griesbachian, slightly stronger recovery during the Dienerian and Smithian, and a strong recovery during the Spathian (Algeo, 2011; Fraiser et al., 2013). However, Hofmann et al. (2011) have suggested that an advanced global recovery occurred during the Griesbachian, and post-Griesbachian events delayed the complete recovery until the Spathian.

The definition of recovery as a return to prior dominance and diversity of a paleocommunity is not an entirely accurate term for the aftermath of the PTME (Dineen et al., 2014). The Early Triassic marks the faunal change from the brachiopod-rich Paleozoic Evolutionary Fauna (EF) to mollusc-rich Modern EF (Gould & Calloway, 1980;

Sepkoski, 1981; Algeo et al., 2011; Dineen et al., 2014). Therefore, the term

"restructuring" would be more apt, as the preceding fauna of the Paleozoic has been

largely replaced and the previous taxonomic and ecologic structure no longer exists

(Dineen et al., 2014).

Groups that suffered most during the aftermath were anthozoans, brachiopods,

bryozoans, cephalopods, and crinoids (Schubert & Bottjer, 1995; Algeo et al., 2011).

During the earliest of the Triassic, a significant reduction in body size, known as the

"Lilliput Effect", occurred in the surviving and newly evolving organisms (Twitchett,

2007; Algeo et al., 2011). Many of these organisms began to return to pre-extinction

size during the Early and Middle Triassic when ecological conditions began to improve

(Algeo et al., 2011).

The Lower Triassic subtidal rock record shows high volumes of flat-pebble

conglomerates, wrinkle structures, microbialites, and carbonate sea floor fans (Pruss et

al., 2005). Subtidal microbialites and carbonate seafloor fans are an indicator of an

unusual ocean chemistry due to episodic pulses of anoxic basin waters, and the

presence of flat-pebble conglomerates and wrinkle structures indicates a long-term

reduction in vertical bioturbation. These factors denote reduced levels of infaunal

bioturbation and unusual ocean chemistry in some regions for possibly five to six million

years following the PTME (Pruss et al., 2005). Anoxic bottom and porewaters have a

strong correlation to an absence of bioturbation or reduction in the depth of

penetration of sediments (Gringras et al., 2011).

During the Early Triassic, select species, considered 'disaster taxa', thrived in the deleterious environments following the PTME. The term 'disaster taxa' refers to generalists that have a large stratigraphic range and are abundant during ecologically stressful events, such as mass extinctions (Fischer and Arthur, 1977). Under actualistic environmental conditions, these disaster taxa are generally far less abundant and found in more restricted environments (Schubert & Bottjer, 1995). The most well-known of these disaster taxa during the Early Triassic are linguilid brachiopods, the bivalve *Claraia,* and microbially induced sedimentary structures (MISS) (Pruss et al., 2004; Pruss et al., 2005).

Microbially Induced Sedimentary Structures:

Description

The general term "microbially induced sedimentary structures" (MISS) includes 17 different types of microbial structures classified by modes of formation including variations in growth, baffling and trapping, binding, and biostabilization (Fig. 2) (Noffke et al., 2009; Gingras et al., 2002).
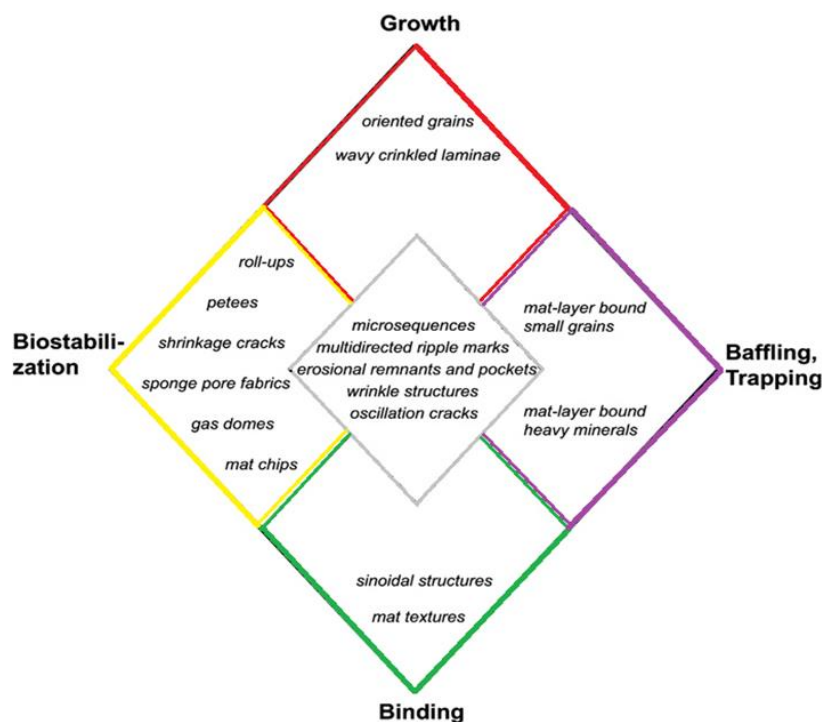
Figure 2. Image showing the 17 different types of MISS classified by their modes of formation. Modified from Noffke, 2009.

While MISS are commonly created from cyanobacteria, they can also be formed by or in conjunction with other filamentous microbes such as green algae, prokaryotic filamentous sulfur oxidizing bacteria, and other heterotrophic bacteria (Bailey et al., 2006; Dupraz et al., 2009). Typically cyanobacteria live near the mat surface along with anaerobic heterotrophs (Pierson et al., 1992; Dupraz et al, 2009). The bacteria, or various microbial filaments, secrete a sticky, extracellular polymeric substance that covers individual sedimentary grains and binds and traps them in a coating known as a biofilm (Decho, 1990; Noffke et al., 2001; Schieber et al., 2007). This baffling and trapping occurs during deposition of sediment, while the binding of sediment and growth occur during periods of no or low sediment influx (Noffke, 2009).

When under optimal conditions, biofilms proliferate and form thick organic layers termed microbial mats. The microbial filaments stabilize the substrate in three ways: sealing sediment by means of a microbial mat, smoothing the rough sediment surface with extracellular mucilages from the microbes, and fixation of loose sediment grains to the mat fabrics (Noffke et al., 2001). Ripple marks are often leveled on a tidal surface by microbial mats as they initially grow in the deeper rippled areas and form planar beds through time. Biostabilization, defined as microbial sediment fixation, also counteracts normal erosional processes (Noffke, 2009; Noffke, 2004). Under normal, actualistic environmental conditions, MISS are restricted to intratidal and deep water due to high infaunalization and sedimentation rates (Noffke, 2004). However, MISS dominated marine subtidal environments in some regions during the Early Triassic (Pruss et al., 2004; Noffke, 2009; Mata and Bottjer, 2012).

Previous Work on Early Triassic MISS

While Lower Cambrian MISS and their associated fossils have been extensively studied, research on Lower Triassic MISS is underrepresented in the literature. Lower Triassic strata in both the western United States and northern Italy produced some of the first global MISS in shallow subtidal siliciclastic paleoenvironments since the Cambrian (Pruss et al., 2004). Pruss et al. (2004) examined wrinkle structures in the Smithian aged Werfen Formation of northern Italy and the Spathian aged Moenkopi and Thaynes Formation in the western United States. The majority of Lower Triassic MISS

studied have come from the Dienerian, Smithian, or Spathian time periods. Little research exists on Griesbachian MISS which directly followed the PTME.

Scientific Significance:

MISS as an Ecological Niche Hypothesis

I hypothesize that MISS provided an ecological niche for some metazoans during the deleterious conditions of the Early Triassic. The two working hypotheses supporting my main hypothesis are that MISS proliferated in the subtidal marine realm during the Early Triassic, and that shelled invertebrates are found in close association with these MISS. My hypothesis will be tested by finding evidence of disaster taxa such as lingulid brachiopods and the bivalve *Claraia* in proximity to the MISS in the Griesbachian rock record. The significant presence of disaster taxa indicates that only select organisms had adaptations to survive the harsh porewater environments created by the microbial mats, creating an ecological niche in which the mats provided a food source and low competition. Additionally, the Lower Triassic rock record shows evidence for the proliferation of microbial mats in subtidal marine settings. While MISS are generally restricted to intratidal and deep water settings due to high infaunalization and sedimentation rates, the Early Triassic provided a unique opportunity for their proliferation.

Contributions of this research

Studying the recovery/restructuring in the Early Triassic can reveal important insight into how biologic and sedimentary systems respond to biotic crisis, specifically in regards to reduction of biotic diversity and long-term environmental fluctuations. While Lower Cambrian MISS and their associated fossils have been studied extensively, research on Lower Triassic MISS is greatly underrepresented in the literature. This insufficient research of Lower Triassic MISS is an important problem because it inhibits our ability to understand the dynamics between changing environmental conditions and its effect on marine communities.

Chapter 2: Geologic Setting

The Griesbachian Dinwoody Formation is exposed across portions of Montana, Wyoming, Utah, Nevada, and Idaho in the western United States (Paull and Paull, 1989). Underlying the Dinwoody Formation is the Permian aged Phosphoria Rock Complex consisting of chert, phosphorite, and limestone (Paull and Paull, 1994). The contact between the Upper Permian and Lower Triassic is unconformable with little evidence of substantial erosion during the lowstand period (Schock, 1981). Because of this unconformity at the Permian-Triassic boundary, the mass extinction event is not recorded (Paull and Paull, 1994).
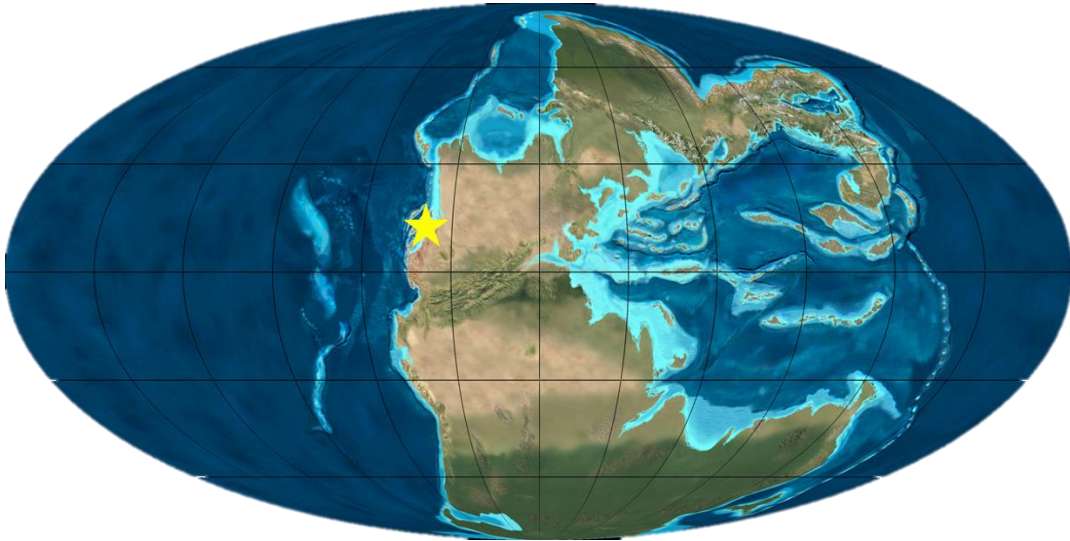
Figure 3. Inferred map of Early Triassic paleogeography (~252 My). Star indicates relative area of study locations on Eastern Panthalassan low-to-mid paleolatitude section. Image modified from Ron Blakely & Colorado Plateau Geosystems, 2011.

The Dinwoody Formation represents a rapid transgression that covered over 270,000 km^2 in the western United States (Fig. 3) (Paull and Paull, 1994). During the highstand and early regression, the Dinwoody Formation was deposited across a flat plain that resulted in deposition of mudstone, siltstone, and limestone. The extent of the Permian Sublett basin was mainly within Idaho with overlap on to adjoining states including: Montana, Wyoming, Utah, and Nevada (Fig. 4) (Paull and Paull, 1994). Subsidence of this basin continued throughout the Early Triassic. The environmental setting throughout the Dinwoody was generally a storm-dominated, distal-to-proximal shelf setting (Paull and Paull, 1983; Rodland, 1999). The maximum thickness of the Dinwoody is 745m in southern Idaho.
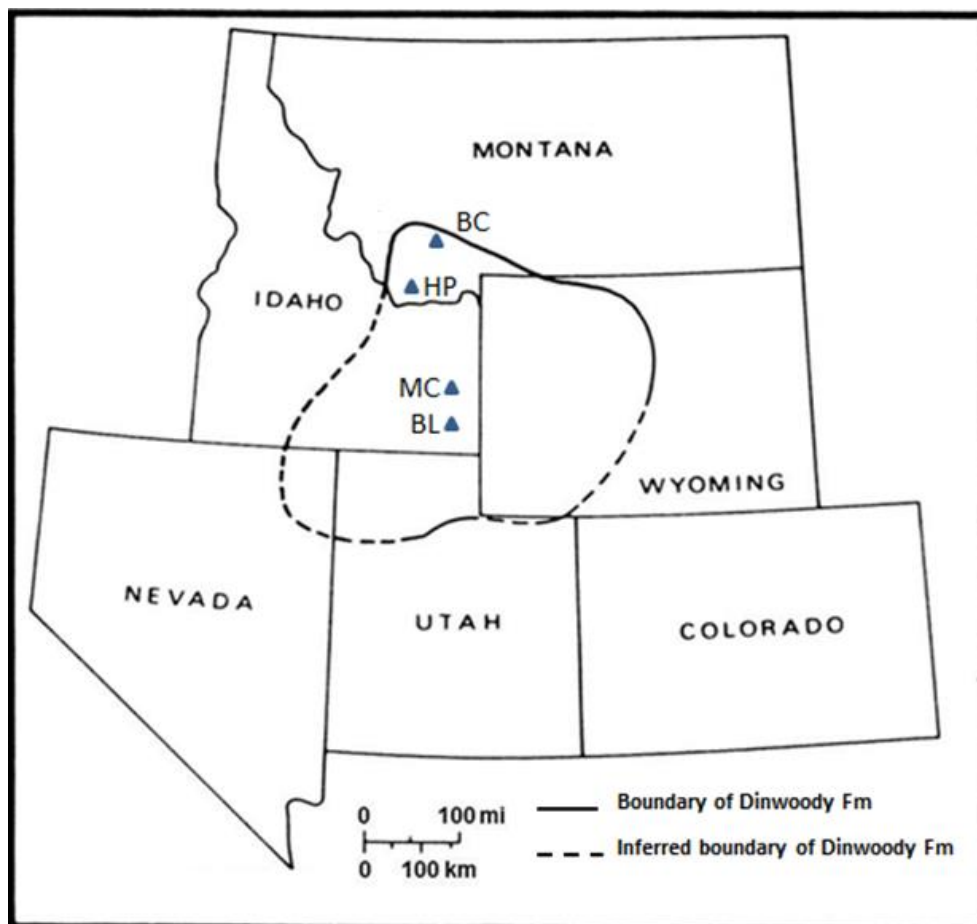
Figure 4. Map of western United States showing boundary and inferred boundary of the Dinwoody Formation during the Griesbachian. Blue triangles indicate localities studied: BC = Blacktail Creek, Montana, HP = Hidden Pasture, Montana, MC = Montpelier Canyon, Idaho, and BL = Bear Lake, Idaho. Image modified from Paull and Paull, 1983

The Dinwoody Formation intertongues and is eventually overlain by the Woodside Formation in the north, east, and southeast (Paull and Paull, 1983). The strata are overlain by the Thaynes Formation; the boundary of which is determined at the base of the cephalopod *Meekoceras*-bearing limestone of the Lower Thaynes

Formation which is approximately 240 million years in age (Paull and Paull, 1983). The study area consisted of four localities in the Dinwoody Formation of the western United States. These localities include: Hidden Pasture and Blacktail Creek in Montana, as well as Montpelier Canyon and Bear Lake in Idaho (Fig. 4) (Schubert & Bottjer, 1995; Schaefer, 2011; Rodland, 1999, Paull and Paull, 1994).

Chapter 3: Methods

Field Methods:

To locate MISS in subtidal marine environments from Griesbachian age strata, the study area consisted of four localities in the Dinwoody Formation. Field work was conducted in May of 2013 with field assistant Jenna Rolle and Dr. Margaret. These localities included: Hidden Pasture and Blacktail Creek in southwestern Montana, and Montpelier Canyon and Bear Lake in southeastern Idaho (Fig. 4) (Schubert & Bottjer, 1995; Rodland, 1999; Schaefer, 2011). Hidden Pasture was selected based on previous work by Schock (1981), which was revisited by Rodland (1999). The Bear Lake and Montpelier Canyon sites in Idaho were previously studied by Schubert & Bottjer (1995) and Schaefer (2011). These localities were selected based on the exposure of the Dinwoody Formation, accessibility, and presence of MISS. The Blacktail Creek locality in Montana was not included in this study because no MISS were found.

Stratigraphic sections of the Dinwoody Formation at each locality were made from the basal unit up the section until the Dinwoody exposure ended. A Brunton compass was used to take the strike and dip of each bed. The thickness of the section

was measured using either measuring tape or a Jacob's staff, depending on terrain and bed thickness. These general measurements were collected and compiled into stratigraphic columns to establish environmental and sedimentological context of the section.

At each locality, samples of bedding planes containing MISS were identified using Schieber et al. (2007) genetic process diagrams from both muddy and sandstone substrates (Fig. 5). These processes for MISS formation include mat growth, metabolism, destruction and decay, and diagenesis of a mat. Processes involving the microbial mats during their life and following their death yield specific features that are identifiable in the field, and are seen on Schieber's diagrams as arrows radiating from the individual process.
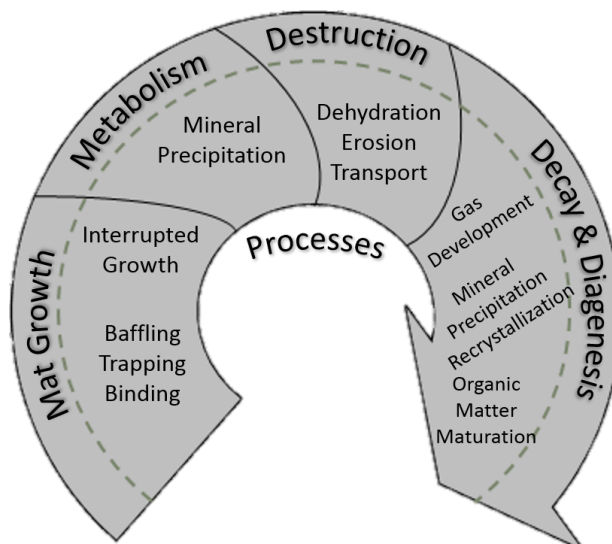
Figure 5. Genetic process diagram for MISS from both muddy and sandstone substrates. Modified from Schieber et al., 2007.

The presence of body and trace fossils, sedimentary structures, and MISS, as well as their proximity to one another in the section, were of particular importance to this study and were incorporated into the stratigraphic columns. The relative abundance of each taxon in the bedding planes were quantified with the terms rare and abundant. Rare was defined as <10 visible body fossils and abundant as >30 visible body fossils per bedding plane. The amount of bioturbation in the bedding planes was quantified using the ichnofabric index (ii) (Droser & Bottjer, 1986). The ii determines the amount of trace fossil activity in a sedimentary rock based off a graded scale of 1-6, with 1 indicating no bioturbation present and 6 indicating over 60% trace fossil coverage of a bedding plane (Droser & Bottjer, 1986).

Lab Methods:

Photogrammetry

Photogrammetry is the use of photographs or other images to capture and measure the spatial relationships of the features of a subject (Breithaupt et al., 2004). The conditions that must be met to make accurate measurements on the photographic images are: 1) two or more photographs taken of the sample that overlap one another approximately 66% and, 2) x, y, z points for three defined points on the overlapping images.
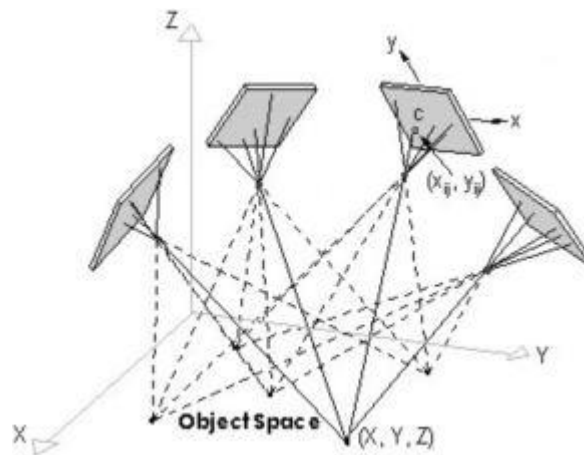
Figure 6. Diagram showing how photogrammetry develops x, y, and z coordinates for
each point and triangulates the aiming angles for each image. Modified from Geodetic
Systems website (http://www.geodetic.com/v-stars/what-is-photogrammetry.aspx).

The x and y points are derived from horizontal measurements on the photos,
while the z point is a vertical value that comes from stereoscopic analysis (Fig. 6). From
the overlapping photographs and defined points, contour maps and 3-D images of the
MISS can be created. The ultimate goal of this method is to create a classification for
different MISS present in the Lower Triassic strata. Breithaupt et al. (2004) used
photogrammetry on dinosaur tracks to show how these computer-generated surfaces
can be studied, measured, and interpreted in new ways.

For the specimens used in this study, the camera was mounted to a stand. A
rigid, non-reflective tray was used to fix the sample and two scale bars to, as to ensure
they maintained a constant position in relationship to one another. The scale bars were
placed perpendicular to one another, to the side and below the sample, and were

elevated to the level of the sample to ensure accuracy of the depth of field. The sample was then lit from above with a Schott Ace light source. The Canon Rebel T3 EOS 1100d camera used was set to an aperture priority of F16, with the settings auto rotation, vibration reduction, and sensor cleaning turned off.

The tray was first positioned so that just the left side of the sample was in the camera's field of view. The tray was then carefully moved in a straight, horizontal line from left to right, taking pictures at every 66% overlap interval. After the series of landscape oriented photos are complete, the tray was then rotated 90 and 270 degrees from the original orientation and the same overlapping photo process is repeated again.

Thin Sections

Three thin sections were created, one each from Hidden Pasture, Montpelier Canyon, and the Bear Lake localities from bedding planes that contained MISS. The purpose of creating these thin sections was to confirm the presence of microbial mediation of the sediments via microscopic characteristics. Alternating dark and light laminations are an indication of MISS due to changes in light intensities from seasonal fluctuations in water depth (Schieber et al., 2007). The dark laminae are primarily filamentous cyanobacteria, while the lighter laminae consist of a combination of coccoid cyanobacteria, extracellular polymers (EPS) and mineral precipitates (Schieber et al., 2007). The EPS trap detrital grains and incorporate them into the microbial mat to aid in vertical growth (Decho, 1990; Noffke et al., 2001). The lighter laminae provide protection for low-light filaments that are below the mat surface in the summer, while

the dark laminae, present in winter, are adapted to decreased light intensity and replace the lighter laminae, creating seasonal layers.

Detrital grains oriented parallel to laminations are important indicators of MISS. To reduce the friction in the matrix, the mat grains orient with their axis parallel to the laminations (Fig. 7) (Schieber et al., 2007). This grain orientation parallel to laminations is characteristic of MISS as gravity-related orientation does not occur in non-microbially mediated laminations.
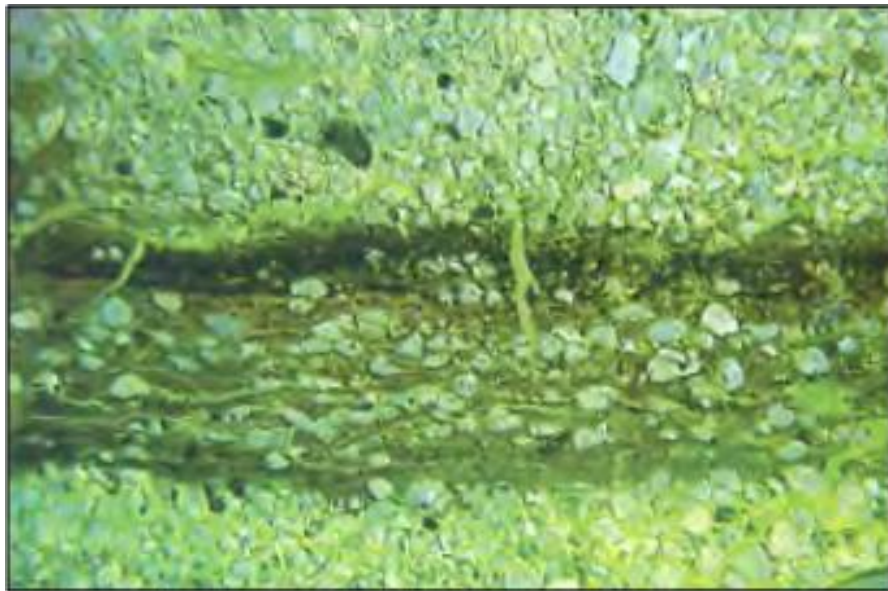
Figure 7. Biolaminate containing matrix-supported sediment grains with their long axes parallel to the laminations. Modified from Schieber et al., 2007.

Additionally, the preferential selection and lamina-specific distribution of heavy mineral grains in MISS is distinctive versus random grain adhesion in non-microbially mediated laminations and is supporting evidence for microbial activity (Schieber, 1999).

The presence of mica grains is also characteristic of MISS, as microbial mats preferentially bind and trap them versus other detrital grains (Schieber et al., 1998; Schieber et al., 2007).

XRF

Determining whether the samples were depleted or enriched of specific trace elements allowed the analysis of the paleoenvironmental redox conditions of the Lower Triassic samples. Seven total siltstone samples containing MISS were examined using X-ray Fluorescence (XRF) analysis: three samples from Montpelier Canyon, two from Bear Lake, and two from Hidden Pasture. The three samples analyzed from Montpelier Canyon were sourced from Bed 1, while both Bear Lake samples were from Bed 3. The two Hidden Pasture samples came from two different beds at approximately 180 m and 224 m.

The samples were prepared using a shatterbox rock crusher, followed by a mortar and pestle to obtain a very fine consistency. All samples were dried overnight in a 105°C oven to remove any excess water. The loss on ignition (LOI) was calculated by heating one gram of each sample in a muffle furnace at 1050 °C for 10 min (methods of McHenry, 2009). Following the XRF techniques and methodology of McHenry (2009), a Bruker S4 Pioneer X-ray Fluorescence (XRF) Spectrometer was used to analyze all seven samples. Ten grams of 50:50 lithium metaborate: lithium tetraborate flux, with a 1% LiBr non-wetting agent, was added to ~1 gram of ammonium nitrate and 1.000 gram of our sample specimen (McHenry, 2009). Using a Claisse M4 fluxer, these mixtures were

fused into glass beads, and then analyzed using a Bruker S4 Pioneer XRF for major, minor, and trace elements (The elements analyzed include Y, Zr, Nb, V, Zn, Ni, Cr, Co, Ce, Sr, Ba, and Mn. A calibration curve for these elements based off of 11 USGS rock standards of sedimentary and igneous rocks of varying compositions was used.

The trace elements vanadium, nickel, and chromium were selected for use in this study because of their redox sensitivity, their common use and prevalence in the literature, as well as their ability to be detected and measured by the XRF (Kloss, 2012). Vanadium is particularly useful when determining redox conditions. It has three oxidation states: V(V) which is stable under oxic conditions, V(IV) which is stable under reducing conditions, and V(III) which is present under reducing, sulfidic conditions (Calvert and Pederson, 1993; Kloss, 2012). Chromium's valence state is affected by changing redox conditions, and nickel is increasingly depleted in marine settings as the seawater becomes anoxic (Kloss, 2012). V, Cr, and Ni concentrations were normalized for this paleoredox analysis by using enrichment factors (EF). The paleoredox ratios of V/Cr and V/(V + Ni) were the preferential equation to normalize the data and complete the paleoredox analysis.

Enrichment factors generally work by comparing the concentration of a trace element in the sample to a concentration commonly used for crustal rocks, or in this case a "standard" shale (Table 1) (Wedepohl, 1971; Tribovillard et al., 2006). Calcium carbonate and opal are often biogenic diluents of the trace elements to be measured. Therefore, EF's are calculated by normalizing the trace element concentration to the aluminum content, which is typically tied to the siliciclastic component of the sediments

and which has very little ability to be lost during diagenesis (Calvert and Pederson, 1993; Tribovillard et al., 2006). The following equation is used to calculate standard enrichment factors:

$$EF_{element\ X} = (X_{sample}/Al_{sample}) / (X_{average}/Al_{average\ shale}). (1)$$

If the EF_X is greater than 1, than the trace element is enriched compared to average shales, and if the EF_X is less than 1, it is depleted (Equation 1) (Tribovillard et al., 2006). Enrichment factor methodology limitations are discussed in Tribovillard et al. (2006).

Elements	Average concentration in seawater (nmol/kg)	Residence time in seawater (kyr)	Average shale (µg/g)
Cr	4.04	8	90
Ni	8.18	6	68
V	39.3	50	130
Al			88,900

Table 1. Geochemical data for trace elements studied (Tribovillard, 2006).

The lower limit of detection (LLD) was also used to assess the quality of the trace element concentration data. Concentrations were analyzed using the following equation: Concentration of trace element (PPM) / (LLD x 2).   Element concentrations were compared to the LLD. If the concentration in PPM (parts per million) was not higher than double the LLD, the value was too low for detection and not used in this study.

Chapter 4: Results: Stratigraphic Analysis

<u>Bear Lake, Idaho:</u>

The Bear Lake measured stratigraphic section consists of 28 m of Dinwoody Formation. The Dinwoody is overlain by the Permian-aged Phosphoria Formation here, indicating the section has been overturned (Fig. 8).

Figure 8. *(Left)* Base of Dinwoody Formation at Bear Lake. Section is overturned, overlying strata is Permian-aged Phosphoria Formation. *(Right)* Top of Dinwoody section at Bear Lake.

The Dinwoody Formation at Bear Lake is composed entirely of light to dark grey siltstone beds throughout the section (Fig. 11). The basal unit is approximately 0.5 m thick and is comprised of finely laminated, dark gray to black shale (Fig. 9). Above the basal unit is 3m of light brown to light red siltstone with laminations as the only visible sedimentary structure. The trace fossil *Planolites* is present but rare, and no other fauna were observed in this portion of the Dinwoody. There was no bioturbation visible, indicating an ii of 1.

Figure 9. Basal unit of Dinwoody at Bear Lake.

A steep sloped, covered interval 10 m thick overlies the basal beds. The top of the Dinwoody Formation at Bear Lake consists of 14 m of highly weathered, laminated siltstone. Lingulid brachiopods and the bivalve *Claraia* occur in these upper beds in moderate abundance with rare trace fossils of *Thalassinoides* and *Planolites,* giving the section an ii of 2. MISS in this unit are rare, and are found with small numbers of lingulids and *Claraia* (Fig. 10)*.*

The only sedimentary structures preserved in this interval were microbially-mediated interference ripples and MISS (Fig. 10).

Figure 10. *(Top)* Sample from top unit of Dinwoody at Bear Lake. Arrows indicate the bivalve *Claraia* and circle indicates MISS on same bedding plane. *(Bottom)* Magnified image of MISS from above image.

Figure 11. Stratigraphic column of Bear Lake, Idaho. Includes ichnofabric indices (ii) chart to the right of the column. Dots on ii graph indicate data points where information was collected.

Interpretation

The Dinwoody Formation at Bear Lake consists entirely of finely laminated siltstone beds that were deposited in middle to outer shelf facies. The lower 3.5 m of the Dinwoody at Bear Lake contains rare trace fossils and dark grey laminations, both of which likely indicate a subtidal setting. The increasing presence of fossils and sedimentary structures in the top 14 m would indicate increasing oxic conditions.

Montpelier Canyon, Idaho:

The Montpelier Canyon stratigraphic section contains approximately 17 m of Dinwoody Formation strata that are overlain by the Thaynes Formation (Fig. 14). The basal unit of this section consists of 9 m of fine-grained, laminated siltstone (Fig. 12).
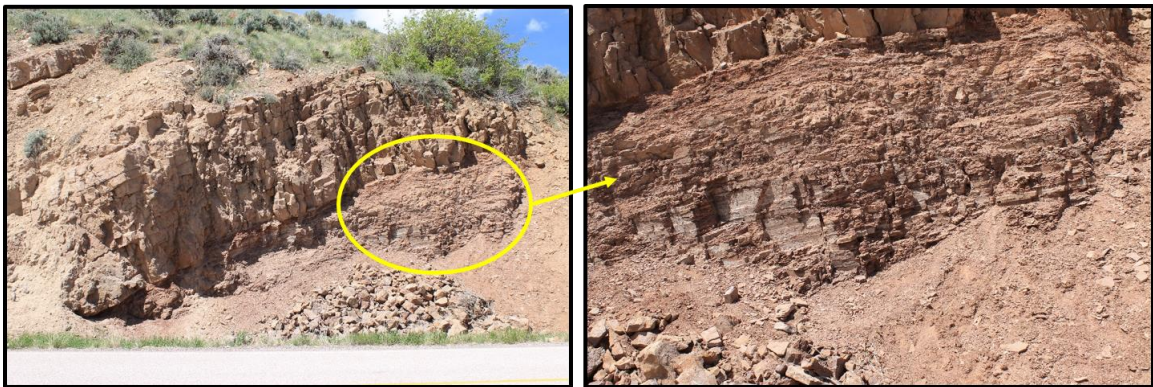
Figure 12. *(Left)* Image of Dinwoody Formation at Montpelier Canyon. Circle indicates basal unit containing MISS. *(Right)* Close up of basal unit of Dinwoody showing laminations and bedding.

The bottom 3 m contains laminations that are highly weathered with rare hummocky cross stratification. This interval contains MISS with rare lingulid brachiopods, *Claraia,* and *Planolites* present on the same bedding planes (Fig. 13).
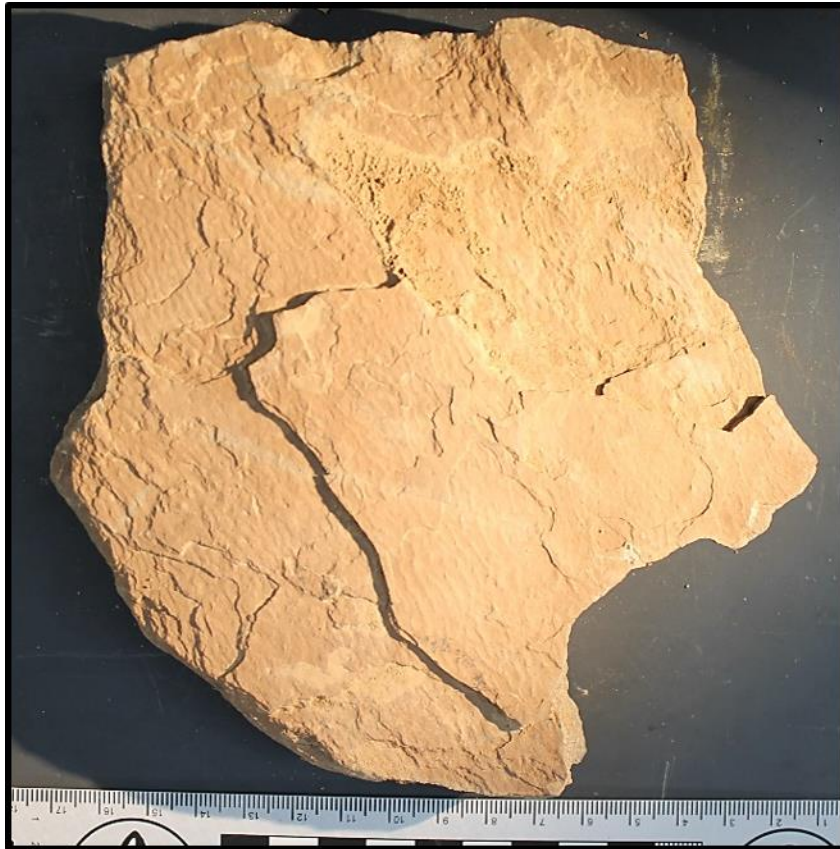
Figure 13. MISS from basal unit of Dinwoody Formation at Montpelier Canyon.

Abundant mica can also be seen on bedding planes associated with MISS, often giving the rocks a slightly blue appearance. The basal interval has an ii of 1 due to an absence of ichnofossils.
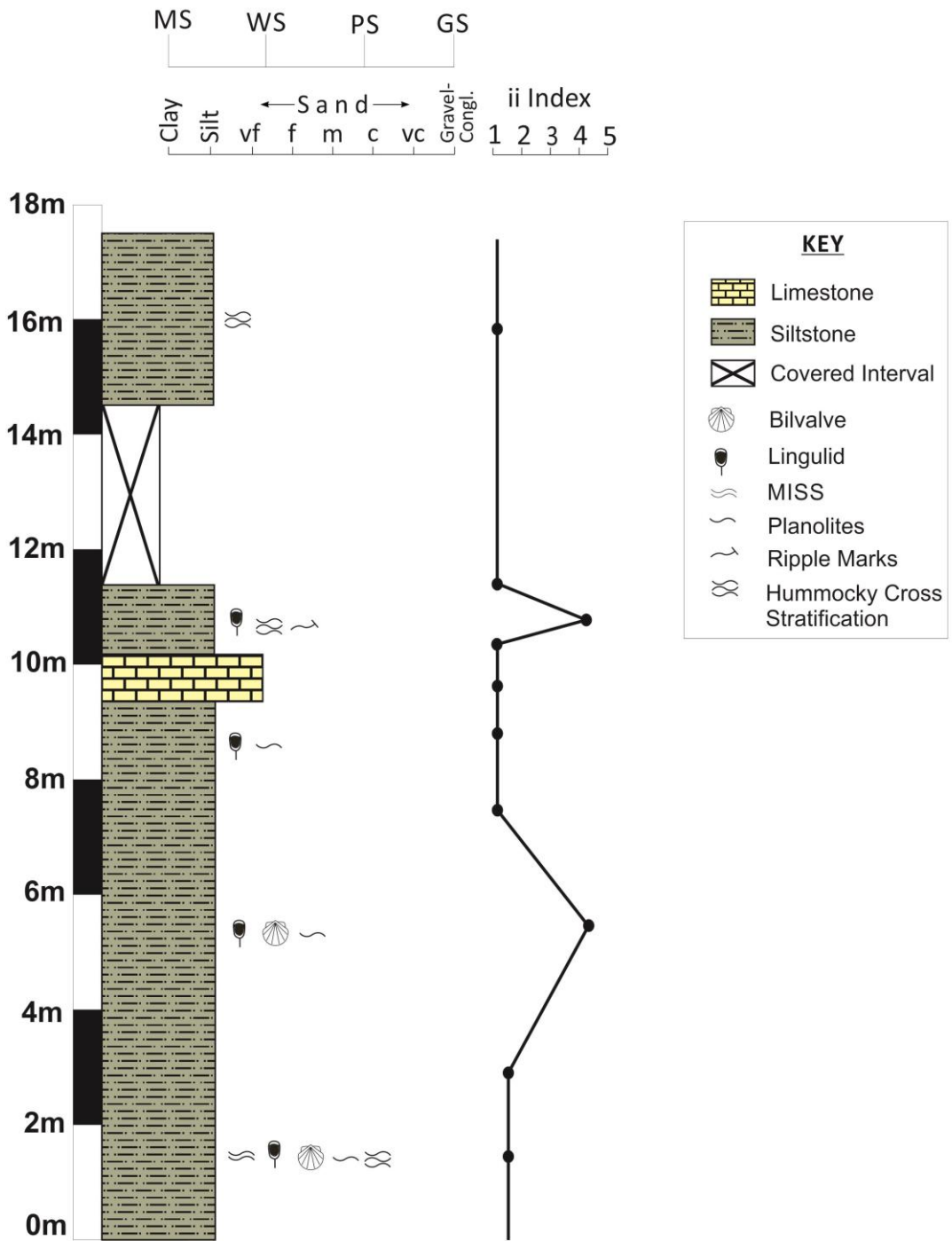
Figure 14. Stratigraphic column of Montpelier Canyon, Idaho. Includes ichnofabric

indices (ii) chart to the right of the column. Dots on ii graph indicate data points where

information was collected.

The overlying interval is 6 m thick and includes abundant lingulid brachiopods, *Claraia,* and the trace fossil *Planolites.* There are no visible sedimentary structures here, possibly due to significant bioturbation with an ii of 4. While no lithological or structural changes occur at the top of this interval, the ii dips significantly to 1 and *Claraia* no longer appear.

Overlying the siltstone is a lithology change to highly weathered limestone that preserved no visible fossils or sedimentary structures. Directly above this weathered limestone layer is a highly bioturbated (ii of 4) siltstone bed with hummocky cross stratification and ripple marks. This siltstone interval is bedded towards the base of the unit with thinner laminations towards the top and rare lingulid brachiopods.

The top of the siltstone bed at 11 m is an area of significant structural deformation that is depicted as a covered interval in the stratigraphic column (Fig. 14). There is likely a fault running through this exposure, as there is evidence of linear deformation of the strata. For the purposes of this study, we did not examine this deformed area. The top bed of the Dinwoody Formation at Montpelier Canyon from 15 to 17 m consists of siltstone, with hummocky cross stratification but no visible fossils.

Interpretation

The Dinwoody Formation at Montpelier Canyon consists primarily of finely laminated siltstone deposited in middle to outer shelf facies. Episodic increases in the ii are loosely associated with hummocky cross stratification and ripple marks, along with an increased fossil presence and the absence of MISS. The lithology of highly

metamorphosed strata from 11-15 m is undeterminable, but a lower limestone interval from 9-10 m, along with the unidentified metamorphosed beds, episodic increases in ii, and intermittent sedimentary structures throughout the formation supports the overall interpretation that these strata were deposited under episodic oxygen increases.

Hidden Pasture, Montana:

The Hidden Pasture section of the Dinwoody Formation is approximately 240 m thick and is overlain by and intertongues with the Woodside Formation. The basal unit of this section consist of 33 m of brown/gray siltstone with laminations that is mostly covered (Fig. 15). *Claraia* and rare lingulid brachiopods occur in this unit, but trenching was required to see these macrofossils *in situ*. Overlying the basal unit is a 20 m mudstone bed that contained abundant *Claraia,* but no other fossils. As in the basal beds, significant trenching was required to obtain fossils *in situ.* There were no other trace fossils, macrofossils, or sedimentary structures found in the lower 53 m of the Dinwoody Formation exposed here, and both units have an ii of 1.

Following an approximately 80m covered interval are alternating limestone beds and covered intervals. The wackestone and packstone beds exposed between 127 m and 145 m contain rare lingulid brachiopods, abundant microgastropods, and abundant bivalves. From 145 m to 147 m, a lithology change to silty limestone occurs, followed by three intervals of exposed limestone units that are increasing in fossil abundance from wackestone to packstone. Bivalves were seen in all four of these units, from 145 m to 175 m, with rare lingulid brachiopods seen in the silty limestone and top limestone unit.
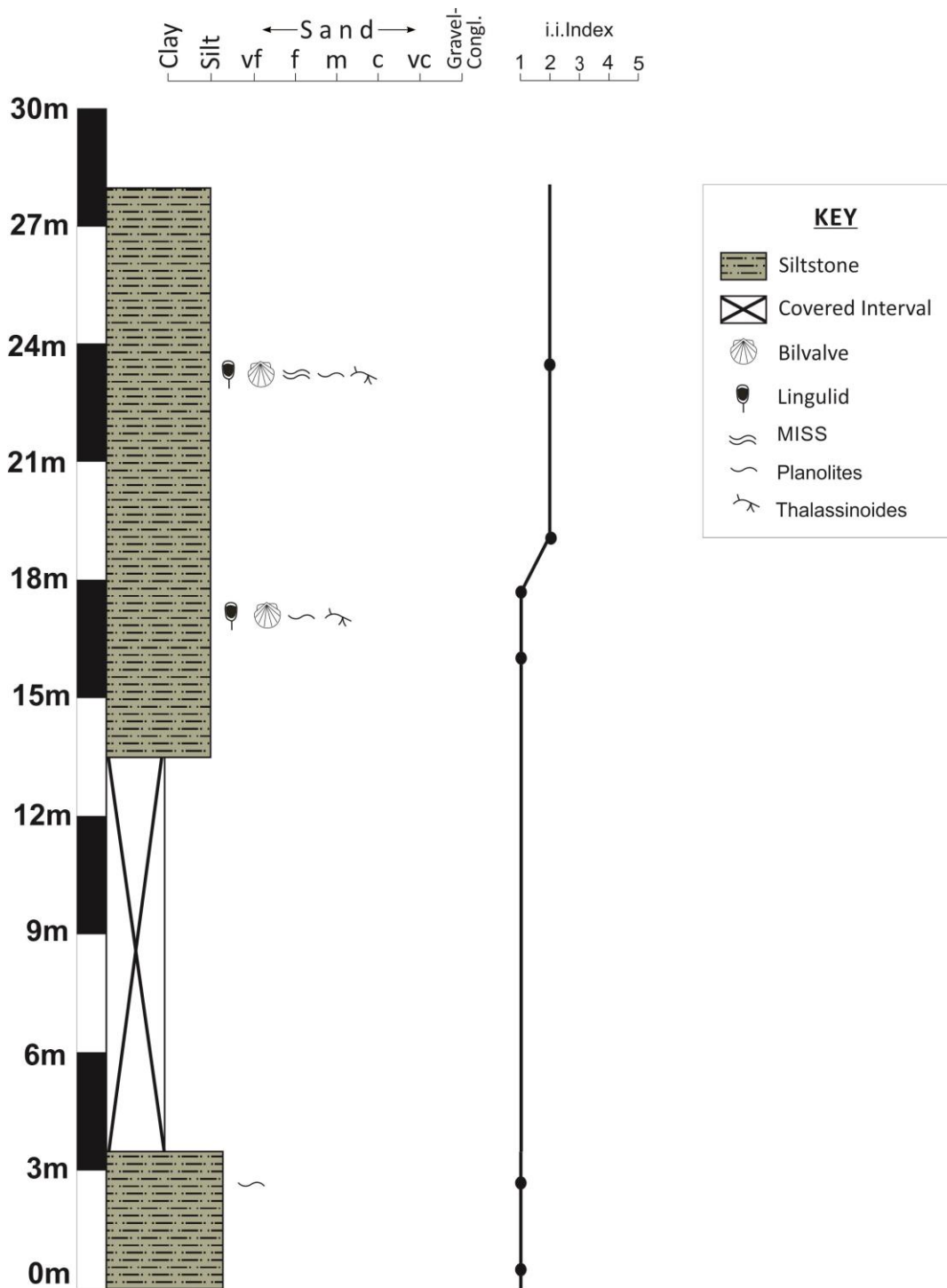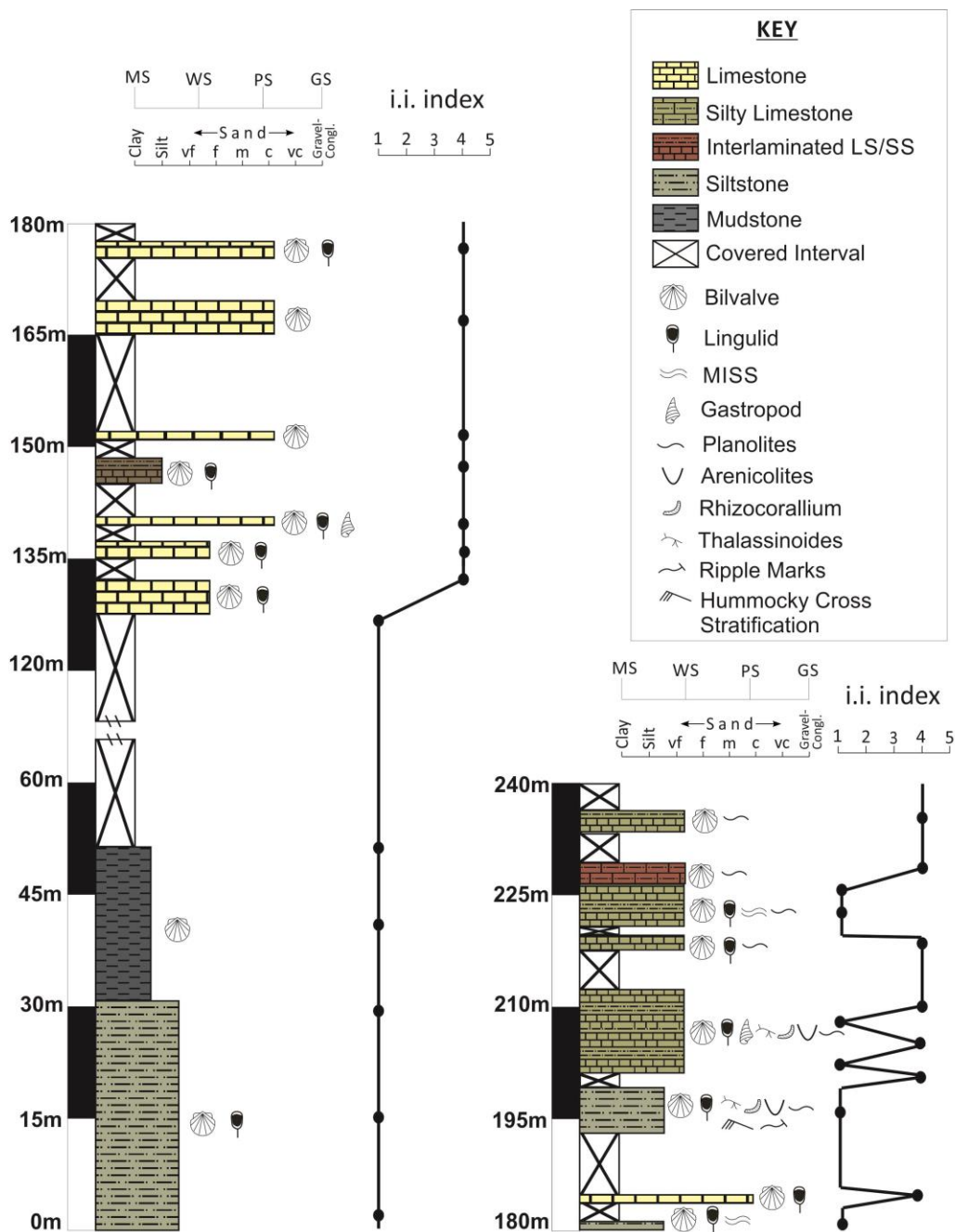
Figure 15. Stratigraphic column of Hidden Pasture, Montana. Includes ichnofabric indices (ii) chart to the right of the column. Dots on ii graph indicate data points where information was collected.

At the 180 m interval, a thinly laminated, 1 m thick siltstone shows the first occurrence of MISS in the Hidden Pasture section (Fig. 16).

Figure 16. MISS from Dinwoody Formation at Hidden Pasture. *(Left)* Found at approximately 180 m and *(Right)* and 225 m respectively.

This unit contains interlaminated packstone with abundant bivalves and lingulid brachiopods, and beds containing MISS with rare lingulid brachiopods. A siltstone interval with a coarsening upward trend starts at 193 m and continues to 245 m upsection. The siltstone unit from 193 m to 199 m contains ripple marks and cross bedding associated with bivalves, lingulid brachiopods, and the trace fossils *Arenicolites, Rhizocorallium, Planolites,* and *Thalassinoides* (Fig. 17)*.*

Figure 17. Ripples from Dinwoody Formation at Hidden Pasture at approximately 195 m.

From 199 m to 240 m, silty limestone units alternate with covered intervals and an interbedded siltstone and limestone unit from 227 m to 229 m. The silty, limestone rich beds contain broken bivalves and lingulid brachiopods in dense packstones, found in association with the trace fossils *Arenicolites, Rhizocorallium, Planolites,* and *Thalassinoides.* The interbedded siltstone and limestone unit from 227 m to 229 m contains bivalve hash and the trace fossil *Planolites,* which is mirrored in the top unit of silty limestone from 234 m to 236 m. However, the top unit changes from packstone, seen in the previous silty limestone beds, to wackestone beds. At approximately 223 m, a reappearance of MISS occurs associated with rare lingulid brachiopods and bivalves. This MISS-bearing bed has an ii of 1, unlike the top 35 m of the section, which displays an ii of 4.

Interpretation

The Dinwoody Formation at Hidden Pasture is representative of the initial transgression and subsequent shallowing during the Griesbachian. This is evidenced by laminated siltstone and mudstone facies lower in the formation associated with the disaster taxa *Claraia* and lingulid brachiopods. From 130-180 m a limestone lithology dominates with a general coarsening upward sequence from wackestone to packstone beds of predominately bivalves, rare lingulid brachiopods, and microgastropods suggesting the package shallowed upward. These alternating beds at top of the Dinwoody Formation at Hidden Pasture indicate a relative stability of the sea level on the shallow shelf among the top 60 m of the Dinwoody at Hidden Pasture (Paull and Paull, 1989).

Significant fluctuations in ii were observed in the top of the formation, alternating sharply between 1 and 4. A general trend of an ii of 1 is seen in the siltstone beds, while the more limestone rich beds have an ii of 4. At 180 m and 224 m, MISS are observed associated with an ii of 1, lingulid brachiopods, *Claraia,* and the trace fossil *Planolites.* These MISS bearing beds are clearly defined from the surrounding beds that have an ii of 4 and increased fossil abundance. These periods of low ii associated with MISS could be directly related to upwelling of the OMZ which would bring anoxic waters onto the shallow shelf, or simply be related to the magnitude of the extinction and its aftermath (Algeo et al., 2010, 2011).

Chapter 5: Results: Photogrammetry

There were several issues encountered using photogrammetry for the first time on this small of a spatial scale. The instructions were created through a series of trial and error between Brent Breithaupt and Neffra Matthews from the Bureau of Land Management and myself. The camera settings were modified for the scale change from their current use on larger-scale features, such as dinosaur tracks, as well as adjustments made based on the variances in cameras used, as each has slightly different settings and features.

Lighting was also an issue encountered when photographing these small scale images. Large scale photogrammetry is used outdoors with sunlight as overhead lighting to capture minute details of the object. On these small scale objects, however, the limited light source available often cast shadows or was not directly above the object to properly illuminate all of the surface features.

The most significant issue encountered was developing a set of photographs that provided the proper orientations of the samples to get sufficient coverage required for photogrammetry. Multiple attempts were made to create a set of photographs with the proper tray orientations to obtain the greatest quality and detailed 3-D images.
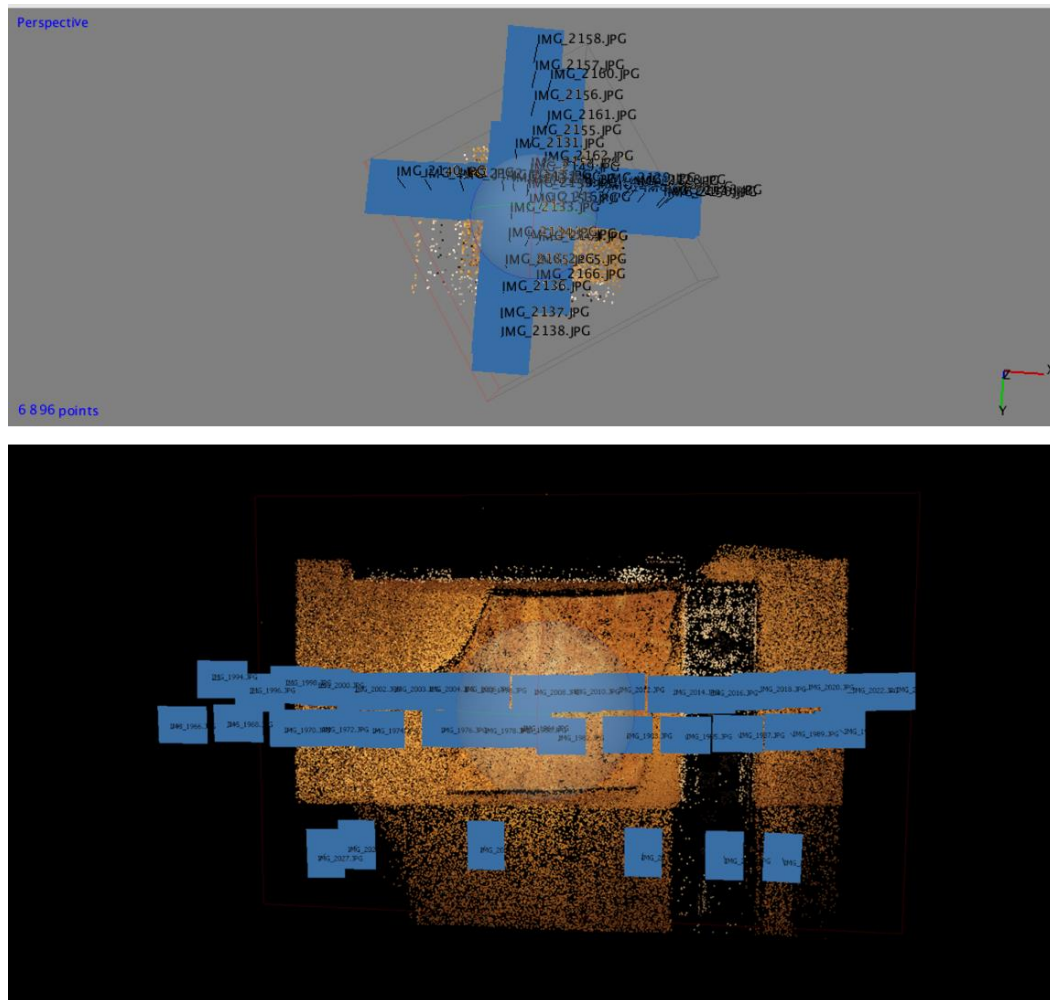
Figure 18. *(Top)* Photogrammetry trial run that produced an image that created a "+" configuration of pictures. The blue boxes represent individual pictures taken. *(Bottom)* Photogrammetry attempt that developed an "H" shaped configuration.

The last trial run produced an image that created a "+" configuration of pictures, which was unsuccessful as it only left a small area of intersection between the two lines (Fig. 18). However, previous attempts had developed an "H" shaped configuration that provided the maximum overlap for deriving camera and lens information (Fig. 18).

Ultimately, we were unable to develop a set of photos that we could take measurements from to classify the MISS in the samples. However, this project is ongoing and collaboration with Brent Breithaupt and Neffra Matthews continues with the eventual goal of publishing our results.

Chapter 6: Results: Thin Sections

Three thin sections, one each from the localities in this study, were examined. The Montpelier Canyon sample exhibited several of the microscopic characteristics associated with microbial mediation. This thin section contained alternating dark and light laminations, wavy to crinkly laminae, detrital grains oriented parallel to these laminations, and the preferential selection of heavy mineral grain adhesion (Fig. 19).
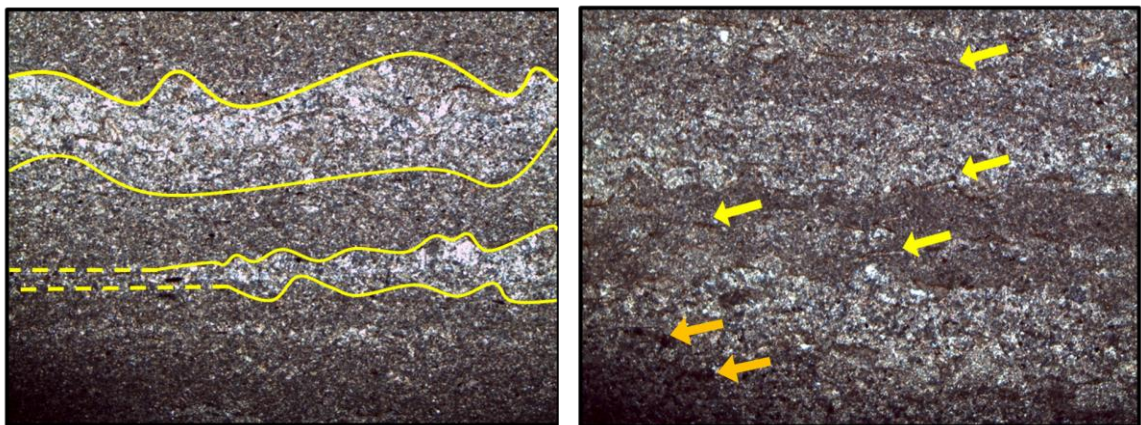
Figure 19. *(Left)* Image of Montpelier Canyon thin section under 10x magnification. Yellow line indicates outline of alternating light and dark laminations. Dashed yellow line indicates inferred boundary of light and dark laminations. *(Right)* Same Montpelier Canyon thin section under 10x magnification. Yellow arrows indicate elongate mica

grains oriented parallel to the crinkles and laminations. Orange arrows indicate altered minerals. Both of these thin sections are from Bed 1 of the Dinwoody Formation at Montpelier Canyon.

The mica grains are elongate with little alteration and are oriented parallel to the laminations. Other minerals were observed in the laminations, but were too heavily altered to determine their original orientation and mineralogy (Fig. 19).
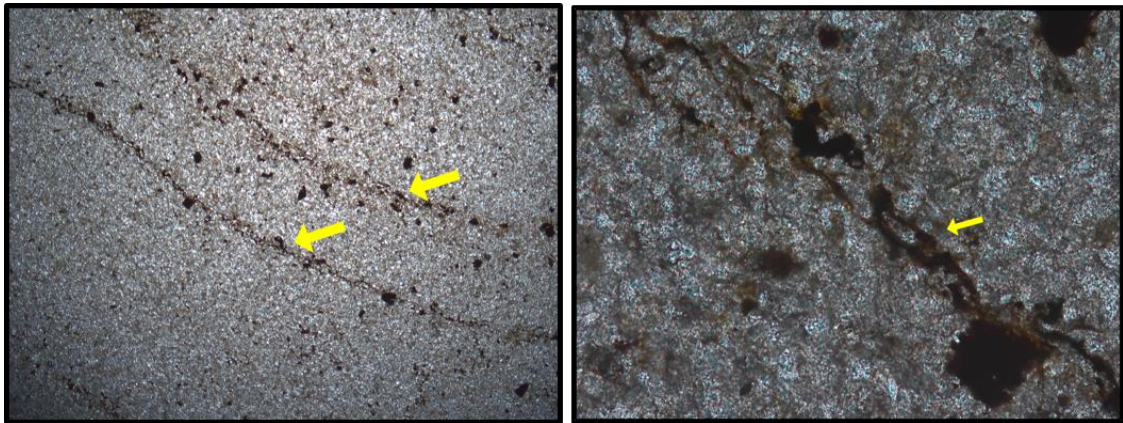
Figure 20. (*Left)* Image of Hidden Pasture thin section under 10x magnification. Yellow arrows delineate highly altered, oblique minerals generally aligned in wavy patterns throughout the thin section. (*Right)* Image of Hidden Pasture thin section under 20x magnification. Yellow arrow shows heavy, highly altered mineral grains in finer detail within the thin section. This thin section was taken from a sample approximately 225 m from the base of the Dinwoody at Hidden Pasture.

Similarly, the Hidden Pasture sample exhibited highly altered mineral grains, potentially from oxidizing and reducing geochemical environments. The mineral grains were too weathered to determine their original orientation and composition. The majority of these heavy, oblique minerals are concentrated in wavy patterns throughout the sample, although some persist in the lighter matrix as well (Fig. 20). It is indeterminate whether these heavy grain patterns constitute laminations and/or indicate microbial mediation.
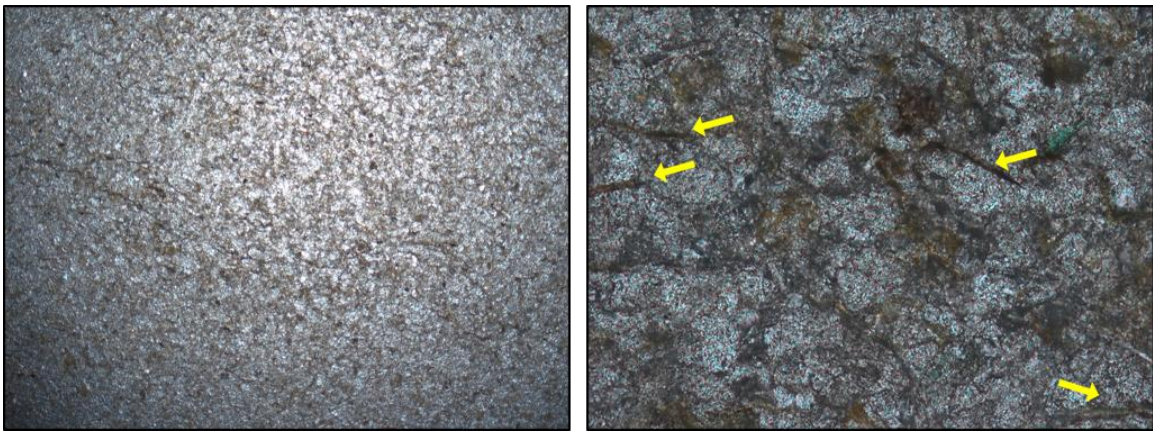
Figure 21. (*Left)* Image of Bear Lake thin section under 10x magnification. (*Right)* Image of Bear Lake thin section under 20x magnification. Yellow arrows indicated mica grains and their general orientation in the sample. Both of these thin sections are from samples approximately 25 m from the base of the Dinwoody at Bear Lake.

Chapter 7: Results: Classification of MISS in the Griesbachian

Three distinct types of MISS were identified in the Lower Triassic strata examined in this study. Hidden Pasture produced MISS identified as multidirectional ripple marks (Noffke et al., 2001; Schieber et al., 2007). These multidirectional ripple marks originally form as ripple marks that are created most commonly by storms, then covered in microbial mats. The final pattern of disordered ripples occurs when the mats continue to develop with episodic disturbance of the sediment, most commonly due to storm activity (Fig. 22) (Noffke et al., 2001).

The thin section created from a Hidden Pasture sample containing MISS shows a series of heavy minerals concentrated in wavy patterns throughout the sample (Fig. 20). It is indeterminate whether these heavy grain patterns constitute laminations and/or microbial mediation in this thin section. However, the physical characteristics of multidirectional ripple marks are consistent with the two samples examined and therefore a classification of MISS can be made.

Figure 22. Multidirectional ripple marks from Hidden Pasture sample.

The Montpelier Canyon locality produced what are considered "classic" wrinkle structures (Fig. 23) (Hagadorn & Bottjer, 1999; Schieber et al., 2007). These are elongate, rounded wrinkle structures that are generally parallel with a moderate crest height. These classic wrinkle structures form from a leveling of ripple marks on a tidal surface (Noffke et al., 2001). The microbial mat will grow preferentially into the troughs of the ripple, over time forming a planar mat surface (Noffke et al., 2001).
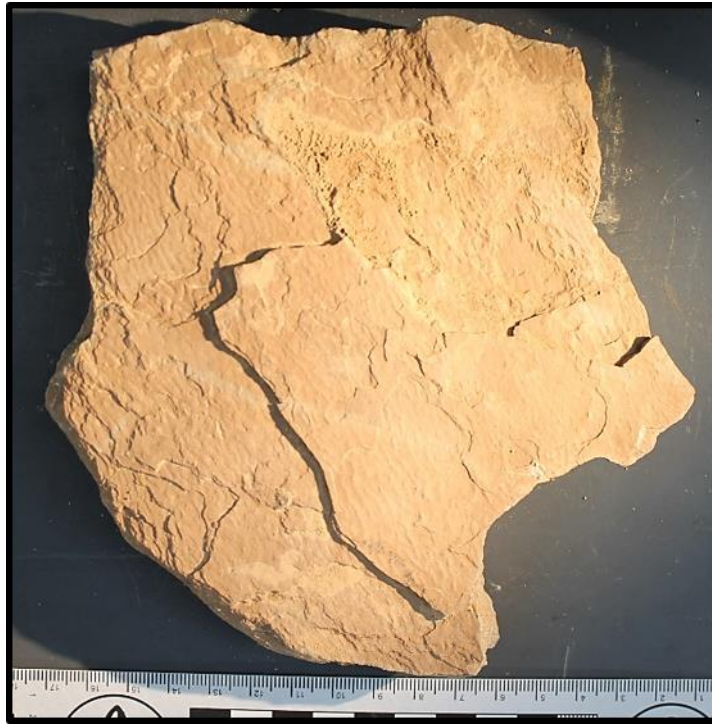
Figure 23. Classic wrinkle structures on Montpelier Canyon sample.

The thin section created from a Montpelier Canyon sample with MISS showed all the classic microscopic characteristics associated with microbial mediation. These include alternating dark and light laminations, wavy to crinkly laminae, detrital grains oriented parallel to the laminations, and preferential selection of heavy mineral grain adhesion. From these microscopic and physical characteristics a definitive classification of MISS can be made for these samples.

The Bear Lake locality produced MISS classified as having a "crinkly" texture (Fig. 24) (Schieber et al., 2007). This texture has polygonal crests and are formed by disruption to the surface of a mat, such as from the impact of moving grains (Schieber et al., 2007).

Figure 24. Crinkly wrinkle structures on Bear Lake sample.

The thin section created from the Bear Lake sample with MISS showed no microscopic characteristics of MISS. However, the physical characteristics of these samples is representative of microbial structures, and therefore can be classified as such.

While only the Montpelier Canyon thin section showed conclusive microscopic characteristics of MISS, one thin section from each locality was not likely representative of the entire stratigraphic section, or even each bedding plane containing MISS. Just as important are the physical definitions of MISS, which all seven samples exhibited some characteristics that enabled that classification.

> **Bedding modified by microbial mats and biofilms**
>
> *Class A: On bedding planes*
>
> 1) leveled depositional surfaces, wrinkle structures
> 2) microbial mat chips
> 3) erosional remnants and pockets
> 4) multidirectional/palimpsest ripples
> 5) mat curls, shrinkage cracks
>
> *Class B: Within beds*
>
> 1) sponge pore fabrics, gas domes, fenestrae structures
> 2) sinoidal laminae
> 3) oriented grains, benthic ooids
> 4) biolaminites, mat-layer-bound grain sizes

Figure 25. Microbially induced phenomena in classification of primary sedimentary structures based off of Pettijohn and Potter (1964). Image modified from Noffke, 2001.

Further, all the samples fall under the classification of primary sedimentary structures following Pettijohn and Potter (1964), including the new category of microbially induced phenomena (Fig. 25) (Noffke et al., 2001). All seven are Class A structures, identified as developing on bedding planes, rather than within beds.

Chapter 8: Results: Geochemical Analysis

Compositional Analysis

The compositional analysis of the seven samples shows mixed carbonate/siliciclastic sediments. Silica (SiO_2) levels ranged from ~ 33% to 58% of the samples' total composition (Table 2). CaO and CO_2 were the other main components at a range of ~ 9% to 30% and ~ 12% to 25% composition respectively.

Sample	MC1-1	MC1-2	MC1-3	BL3-1	BL3-2	HP6-1	HP7-1
SiO$_2$	32.88%	47.55%	33.12%	57.50%	45.52%	47.87%	46.31%
TiO$_2$	0.34%	0.50%	0.32%	0.27%	0.27%	0.54%	0.41%
Al$_2$O$_3$	6.78%	5.83%	6.08%	7.26%	6.75%	12.02%	5.67%
Fe2O3	2.24%	2.03%	2.05%	1.58%	2.11%	4.57%	1.86%
MgO	2.41%	1.62%	2.29%	1.74%	2.25%	4.42%	1.69%
CaO	28.34%	21.09%	29.89%	13.09%	20.66%	8.86%	21.56%
Na$_2$O	0.83%	1.12%	0.97%	2.69%	2.06%	0.63%	1.05%
K$_2$O	1.52%	1.57%	1.20%	0.97%	0.92%	3.32%	1.52%
P$_2$O$_5$	0.16%	0.23%	0.15%	0.13%	0.12%	0.17%	0.24%
CO$_2$	24.22%	12.21%	24.91%	12.54%	18.62%	18.17%	18.73%
Mn	0.10%	0.65%	0.12%	0.06%	0.20%	0.05%	0.70%
V	48	ND	ND	ND	ND	90	ND
Cr	44	41	39	ND	22	62	34
Zn	ND	62	45	ND	ND	87	66
Sr	190	189	193	164	212	123	169
Zr	112	409	109	75	78	114	287
Ba	148	225	147	358	1195	287	185
Ce	128	177	151	ND	ND	155	166
Sum (%)	99.90	94.53	101.17	97.91	99.66	100.72	99.84
LOI	24.22%	12.21%	24.91%	12.54%	18.62%	18.17%	18.73%

Table 2. Major elements of the carbonate/siliciclastic samples tested in this study (XRF).
Results reported at wt% oxide except V, Cr, Zn, Sr, Zr, Ba, and Ce, which are reported in
PPM (parts per million) (McHenry, 2009). Sample name indicates locality and sample
number. MC = Montpelier Canyon, BL = Bear Lake, and HP = Hidden Pasture.

Trace Element Concentrations

 Nickel. Nickel was only detected in high enough concentrations in one of the
samples from Hidden Pasture. This sample only showed very minute amounts of the

trace element, at 34 parts per million (PPM), and therefore the paleoredox ratio of V/(V + Ni) was not used in this study.

Vanadium. The trace element Vanadium was only detectable in two samples at high enough concentrations to be measured. In a sample from Montpelier Canyon (MC1-1) the V concentration was 48 PPM with an EF of 0.91 and a sample from Hidden Pasture (HP6-1) the concentration was 90 PPM with an EF of 0.97 (Table 3). Both of these EF's are below 1, indicating that these samples are depleted of Vanadium. The paleoredox ratio of V/Cr was used for the two samples with high enough detection, indicating 1.09 for the Montpelier Canyon sample and 1.45 for the Hidden Pasture sample. These two ratios are indicating reducing conditions.

Chromium. The trace element Chromium was detected in high enough concentrations in six of our seven samples. These concentrations range from 22 PPM to 62 PPM (Table 3). Initially the paleoredox ratio of V/Cr was the preferential equation to normalize the data and complete the paleoredox analysis. While six of the seven samples contained Chromium high enough to obtain substantial data, only two samples of Vanadium were at detectible levels, making any results of the normalization weak. Calculating 4 of the 6 samples has shown an EF above 1, which would indicate these samples are enriched with chromium (Table 3).

Sample	Al (PPM)	Cr (PPM)	Enrichment Factor (EF) of Cr	V (PPM)	Enrichment Factor (EF) of V	Paleoredox Ratio V/Cr
MC1-1	35,887	44	1.22	48	0.91	1.09
MC1-2	30,858	41	1.30	ND		
MC1-3	32,181	39	1.20	ND		
BL3-1	38,427	ND		ND		
BL3-2	35,728	22	0.62	ND		
HP6-1	63,622	62	0.97	90	0.97	1.45
HP7-1	30,011	34	1.12	ND		

Table 3. Enrichment factor values for vanadium and chromium.

The values given (Table 4) show that any value beneath 100% of the sample was below

detection rate; these values are marked in red. Common trace elements that were in

concentrations too low for detection for all or most samples were Nb, Co, Ni, and V.

Sample	Element	Concentration (PPM)	Stat. Error	(LLD)	Concentration /2x LLD (%)
DWMC1-1					
	Y	28	13.60%	4	393%
	Zr	112	4.00%	12	482%
	Nb	11		10	56%
	V	48	11.50%	18	135%
	Zn	38	12.60%	18	106%
	Cr	44	4.24%	11	196%
	Co	9	17.80%	14	31%
	Sr	128	8.54%	59	108%
	Ba	190	3.42%	16	608%
	Mn	148	10.50%	54	139%
DWMC1-2					
	Y	25	17.60%	4	358%
	Zr	409	1.25%	12	1762%
	Nb	18	138.00%	10	95%
	V	24	16.00%	19	65%
	Zn	62	9.39%	18	174%
	Ni	1	10.10%	14	5%
	Cr	41	4.38%	11	181%
	Co	7	20.00%	15	24%
	Ce	177	6.37%	63	140%
	Sr	189	3.25%	15	619%
	Ba	225	7.93%	55	205%
	Mn	0	0.81%	223	
DWMC1-3					
	Y	27	14.10%	4	387%
	Zr	109	4.07%	12	472%
	Nb	18	158.00%	10	92%
	V	38	13.90%	18	107%
	Zn	45	11.60%	18	124%
	Cr	39	4.44%	11	173%
	Co	9	18.80%	14	30%
	Ce	151	7.80%	59	129%
	Sr	193	3.35%	16	618%
	Ba	147	10.60%	54	137%
	Mn	0	1.04%	95	
DWBL3-1					
	Y	21	32.40%	3	306%
	Zr	75	5.60%	11	329%
	Nb	14		10	74%
	V	26	17.90%	17	78%
	Zn	28	13.90%	17	83%
	Ni	5	9.65%	14	18%
	Cr	39	9.53%	24	81%
	Co	8	22.10%	15	26%
	Ce	112	6.10%	68	83%
	Sr	164	3.29%	15	565%
	Ba	358	5.55%	52	346%
	Mn	0	1.76%	100	

Sample	Element	Concentration (PPM)	Stat. Error	(LLD)	Concentration /2x LLD (%)
DWBL3-2					
	Y	22	24.80%	4	318%
	Zr	78	5.25%	12	337%
	Nb	8		10	41%
	V	18	23.60%	17	51%
	Zn	37	12.50%	18	106%
	Ni	3	9.97%	14	9%
	Cr	22	5.04%	11	100%
	Co	16	15.00%	15	54%
	Ce	73	2.92%	81	45%
	Sr	212	2.83%	15	703%
	Ba	1195	2.15%	52	1142%
	Mn	0	1.58%	217	
DWHP6-1					
	Y	26	15.10%	3	385%
	Zr	114	4.02%	11	519%
	Nb	14		10	74%
	V	90	6.43%	18	250%
	Zn	87	7.16%	17	252%
	Ni	24	7.94%	15	79%
	Cr	62	7.72%	25	125%
	Co	18	9.61%	16	55%
	Ce	155	5.94%	67	116%
	Sr	123	5.20%	15	410%
	Ba	287	6.21%	53	270%
	Mn	0	1.95%	102	
DWHP7-1					
	Br	20	35.90%	4	291%
	Y	287	1.71%	12	1249%
	Zr	18	159%	10	92%
	Nb	26	16.00%	18	73%
	V	66	8.85%	18	188%
	Ni	34	4.57%	11	154%
	Cr	20	14.20%	14	69%
	Co	166	6.95%	61	135%
	Ce	169	3.54%	15	560%
	Sr	185	8.82%	53	174%
	Ba	0	0.77%	224	
	Mn	0	0.77%	224	

Table 4. Trace element concentration, statistical error, and concentration versus twice LLD. LLD units is PPM (parts per million). Elements below detection are marked in red.

Chapter 9: Results: MISS and their Associated Fossils

The three localities observed in this study all contain MISS consistently associated with the same lithological characteristics and fossil assemblages. Each bedding plane containing MISS was composed of siltstone deposited in middle to outer shelf settings. Additionally, at both Hidden Pasture and Montpelier Canyon the ichnofabric indices associated with the bedding planes containing MISS was 1 (the Bear Lake locality the ii was 2, indicating that bioturbation was either entirely absent, rare, or primarily horizontal in bedding planes with MISS. All three localities show a low ii in their siltstone beds.

The associated fossils and abundances of fossils are distinct in bedding planes containing MISS versus ones without. Lingulid brachiopods and the bivalve *Claraia* are found in every bedding plane containing MISS. Linguilids and the bivalve *Claraia* are both well adapted to low-oxygen environments which are generally associated with MISS (Wignall, 199X; Schubert & Bottjer, 1995; Rodland & Bottjer, 2001). While both of these taxa are found also in bedding planes not containing MISS, their abundance is far lower in the MISS beds versus other siltstone bedding planes.

The trace fossils *Planolites* and *Thalassinoides* are the only ichnofossils found associated with bedding planes containing MISS in this study. *Planolites* is a simple, horizontal burrow that is a common feeding trace found in Lower Triassic strata (Table 5) (Pruss et al., 2004). *Thalassinoides* is the only other trace fossil found associated with MISS and is a branching trace with either horizontal or shallow vertical burrows (Pruss et al., 2004). These trace fossils are rare in the Griesbachian, increasing in diversity and

abundance from the earliest to late Early Triassic, and indicate metazoan behaviors in the earliest part of the recovery (Pruss et al., 2004).

Age	Formation	Location	Ichnotaxa	References
Spathian	Moenkopi, Virgin Limestone Member	Western US	*Arenicolites Asteriacites Gyrochorte Laevicyclus Planolites Rhizocorallium Thalassinoides*	Pruss et al. (2004)
Dienerian/ Smithian	Moenkopi, Sinbad Limestone Member	Western US	*Arenicolites Diplocraterion Planolites Rhizocorallium*	Fraiser (2000)
Griesbachian	Dinwoody	Western US	*Planolites*	Twitchett and Barras (2004)
Griesbachian	Toad	Western Canada	*Cruziana Palaeophycus Planolites Rusophycus Thalassinoides*	MacNaughton et al. (2002)
Griesbachian	Montney	Western Canada	*Chondrites Cruziana Cylindrichnus Diplocraterion Phycodes Phycosiphon Planolites Protovirgularia Rhizocorallium Rosselia Skolithos Spongeliomorpha Thalassinoides Treptichnus*	Zonneveld et al. (2002)

Age	Formation	Location	Ichnotaxa	References
Griesbachian	Dinwoody	Montpelier Canyon, ID Bed 1	*Planolites*	This paper
Griesbachian	Dinwoody	Bear Lake, ID Bed 3	*Planolites Thalassinoides*	This paper
Griesbachian	Dinwoody	Hidden Pasture, MT 180 m	None	This paper
Griesbachian	Dinwoody	Hidden Pasture, MT 224 m	*Planolites*	This paper

Table 5. *(Top)* Table showing Lower Triassic trace fossils studied in North America and western Canada (Modified from Pruss et al., 2004). *(Bottom)* Table showing location of MISS bedding planes and the associated trace fossils.

The MISS examined in the three locations for this study all have similar characteristics, associations, and environments.   While the MISS in each locality are classified differently, they all encompass the physical characteristics attributed to MISS by Pettijohn and Potter (1964) and Noffke (2001). The Montpelier Canyon thin section also showed evidence of microbial mediation through alternating dark and light laminations, wavy to crinkly laminae, detrital grains oriented parallel to these laminations, and the preferential selection of heavy mineral grain adhesion.

Additionally, the MISS are consistently found associated with the same fossil assemblages of disaster taxa and low ii, as well as similar lithological and environmental settings. Each unit containing MISS examined was primarily composed of finely laminated siltstone deposited in middle to outer shelf facies with a bottom water signal showing oxic to suboxic conditions.

Chapter 10: Discussion

Environmental Implications of MISS Following the PTME

Modern microbial mats that are composed of heterotrophic microbes consume oxygen by remineralizing organic material from the overlying water column and from the mat itself (Froelich et al., 1979; Reimers and Suess, 1983; Bender and Heggie, 1984; Bailey et al., 2006). Microbial respiration also consumes oxygen from oxygenic phototrophs at the mat surface as well as the water column. Anoxia can potentially then reach the mat surface even if the overlying water column is oxygenated (Jørgensen and Revsbech, 1985).

If modern microbial mats are used as a proxy for Early Triassic ones, it can be deduced that these microbial communities would have created anoxic conditions < 2mm below the sediment/water interface during the day and at the interface at night (Jørgensen et al., 1992; Bailey et al., 2006).
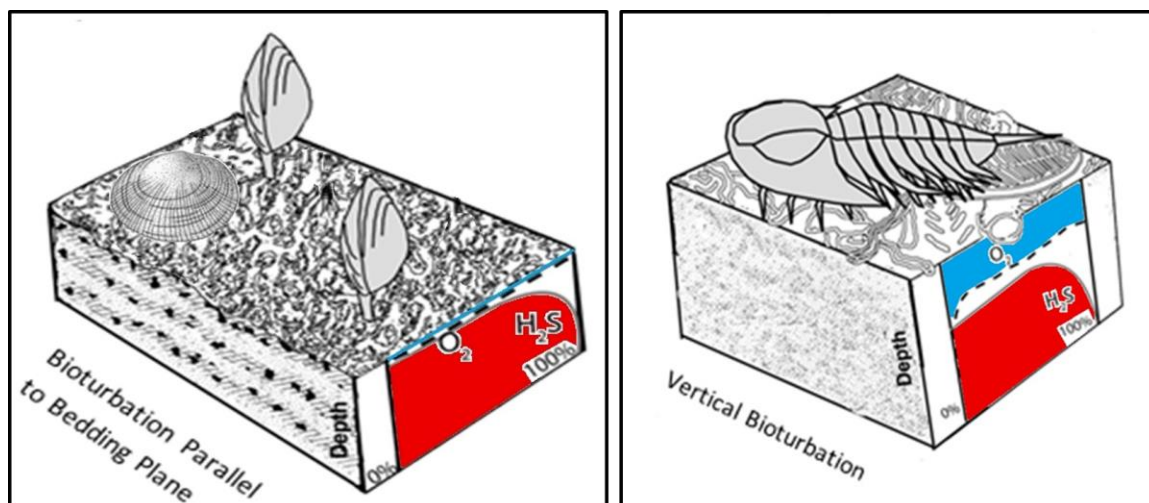
Figure 26. *(Left)* Sediment profile with microbial mat containing lingulid brachiopods and the bivalve *Claraia.* Blue indicates oxygenated porewaters and red indicates hydrogen sulfide rich porewaters versus depth. Within 1-2 mm of surface, oxygen disappears and is replaced by hydrogen sulfide, which decreases as it nears the surface and becomes oxidized. Side view of sediments shows little to no vertical bioturbation due to the hydrogen sulfide rich sediments. *(Right)* Sediment profile not containing a microbial mat. Blue indicates well oxygenated porewaters deeper versus a mat covered sediment. Hydrogen sulfide in red is constrained to deeper in the sediment as its concentration is inversely related to the amount of oxygen present. Side view of the sediments show they are highly bioturbated due to elevated oxygen levels. Modified from Bailey, 2006.

The concentration of oxygen in the porewaters is inversely related to the concentration of hydrogen sulfide, which is oxidized as it reaches the sediment surface (Fig. 26) (Bailey et al., 2006). The hydrogen sulfide in the sediments is produced through bacterial sulfate reduction (Meyer et al., 2008).

Since the porewaters containing microbial mats were likely anoxic, the hydrogen sulfide could potentially have reached the sediment-water interface (Bailey et al., 2006). The proliferation of microbial mats would have created anoxic and euxinic porewaters and made vertical bioturbation physiologically difficult (McIlroy and Logan, 1999).

Following the PTME, the Griesbachian was a time of ecological stress as evidence suggests widespread marine anoxia, euxinia, and hypercapnia in the water column (Luo et al., 2011; Brennecka et al., 2011; Algeo et al., 2011). These ecological barriers to faunal recovery were likely exacerbated by the physiologically stressed benthic environments created by the proliferation of microbial mats.

MISS were found in three of the four localities examined in this study. While this is only a small cross section of the Griesbachian strata in the western United States, the common presence of MISS in subtidal environments at the localities studied leads to the conclusion that MISS proliferated during the Early Triassic. There is also the consideration that MISS are not always preserved due to a small taphonomic preservation window that must be met, so the absence of MISS does not necessarily mean they were not present.

Geochemical Evidence Against Anoxia

C*hromium.* The EF's for 4 of the 6 samples of chromium show that the bottom waters containing MISS are reducing. Tribovillard (2006) states that under normal ocean conditions the chromate anion is soluble, but Cr(IV) is reduced to Cr(III) under anoxic conditions and is transported into the sediments. However, Cr transport and enrichment are very complex and often reduce the limit of its paleoenvironmental utility (Tribovillard, 2006). The paleoredox ratio of V/Cr was the preferential equation to normalize the data and complete the paleoredox analysis. However, only two samples of Vanadium were at detectible levels, making any results of the normalization weak.

Vanadium. The lack of V in five of the seven samples, coupled with EF's of less than 1 for the two samples that did have detectable V, both indicate that there are not reducing conditions in these bottom waters. Redox sensitive elements like V and Ni are deposited preferentially under these reducing conditions (McHenry, 2014). While the average shale concentrations have their shortcomings as stated above, and the two V/Cr ratios indicated reducing conditions, the overall evidence that the V concentrations are so far below the EF standard indicates that this element was not being concentrated in anoxic sediments (McHenry, 2014).

Nickel. Nickel was an integral trace element to use in our study as it is increasingly depleted in reducing sediments and cycled into the overlying bottom waters (Tribovillard, 2006). Only one sample contained high enough concentrations of Nickel for measurement. Such low levels of nickel would indicate that the bottom waters are oxic and that without reducing conditions, Nickel fixation within the

sediments could not take place. In the initial phases of the study, the use of the equation V/(V+Ni) was ideal to normalize the data for this paleoredox analysis. However, since only one sample contained enough and in such a minute amount, this ratio of paleoredox indices was abandoned for the use of EF's.

Also a factor in this study is that these samples are largely composed of carbonate material. The paleoredox studies are not as well adapted to a carbonate component, and carbonate rock samples herein are compared to the average shale value. The normalization to Al is to our benefit, as it correlates to the more detrital and non-carbonate component (McHenry, 2014). Future XRD analysis will be conducted to see the carbonate component more clearly, and make adjustments for a more accurate picture.

The geochemical analysis performed on the seven samples indicate that the bottom water signals associated with MISS were oxic to suboxic. The Vanadium's EF's of <1 for all the samples, combined with an absence of Nickel and undetectable limits for many other redox sensitive elements, leads to the conclusion that the bottom waters were not reducing. While Chromium in 4 of 7 samples showed EF's greater than 1, indicating reducing conditions, Cr transport and enrichment can be very complex and is most accurate when normalized with the paleoredox ratio of V/Cr (Tribovillard et al., 2006). Only two samples of Vanadium were at detectible levels, not only making any interpretations of a normalization of Chromium weak, but this absence supports the oxic to suboxic interpretation of these bottom waters. These geochemical proxies only

indicate the extent that bottom waters of sediments containing MISS were oxic and do not indicate if the porewaters were oxic versus anoxic.

Opportunism and Disaster Taxa

MISS, lingulid brachiopods, and the bivalve *Claraia* are all characterized as disaster taxa for their ability to proliferate in environments where conditions are deleterious to most animals (Fischer and Arthur, 1977; Pruss et al., 2004; Pruss et al., 2005). The opportunistic nature of these organisms allows them to fill niches left vacant from events such as mass extinctions. Opportunists are organisms that thrive and increase in abundance during a recovery period, but return to lower levels of abundance subsequently (Hallam & Wignall, 1997; Rodland & Bottjer, 2001). Disaster taxa are a type of opportunist that overrun vacated ecospaces during recovery periods, but are subsequently forced into marginal settings when the recovery gains momentum (Hallam & Wignall, 1997; Bottjer, 2001; Rodland & Bottjer, 2001).

The restricted presence of MISS before the extinction, proliferation following the PTME, and subsequent retreat after the recovery is characteristic of the opportunistic nature of disaster taxa. Accordingly, microbial communities have dominated the subtidal realm only sporadically throughout geologic history. During the Early Cambrian, microbial communities dominated due to a lack of competition and extensive bioturbation prior to the Cambrian radiation (Bailey et al., 2006). This period of domination is not an example of opportunistic behavior as no competition for ecospace yet existed.

Evidence exists for microbial communities dominating subtidal environments during the recovery of the End Ordovician, End Devonian, and End Permian mass extinctions (Mata & Bottjer, 2012). The End Triassic and End Cretaceous extinctions have not yet been associated with the expanse of microbial communities (Mata & Bottjer, 2012). The two important factors that facilitated these proliferations are low bioturbation and vacant ecospace resulting from these mass extinctions. The scarcity of benthic faunas allowed the microbial communities to dominate in environments where during stable ecological conditions they are outcompeted.

Certain disaster taxa, such as lingulid brachiopods and the bivalve *Claraia*, were able to overcome the physical obstacles the microbial mats created and utilize them as an ecological niche. Although the hydrogen sulfide that the mats produce is toxic to most metazoans, many modern infaunal animals have found ways to reduce the toxicity by using chemoautotrophic bacteria to oxidize the hydrogen sulfide (Bailey et al., 2006). The blood of several varieties of modern inarticulate brachiopods contains a non-heme respiratory pigment called hemerythrin, which enables the storing and transporting of oxygen (Manwell, 1960; Bailey et al., 2006). This ability allows lingulid brachiopods to survive in oxygen-deficient and euxinic conditions. This survival adaptation has been observed in modern brachiopods that are able to survive for several days in a hypoxic setting (Brunton, 1982; Bailey et al., 2006).

Lingulid brachiopods originated in the Early Cambrian and are extant. They are burrowing organisms that attach to the sediment via a long pedicle (Zhang et al., 2004). During geologic intervals of ecological and environmental calm, lingulid brachiopods are

generally restricted to stressed settings such as marginal marine environments and low oxygen conditions (Schubert & Bottjer, 1995). They have retained these defining characteristics with only minor morphological changes since the Early Cambrian, as evidenced by their quality soft-bodied preservation in the Chengjiang Lagerstätte in Southwest China (Zhang et al., 2004). This morphological consistency is important as they are found on microbial mats in both the Early Cambrian and Early Triassic. Their specialized adaptation to hydrogen sulfide and low oxygen perhaps allowed them to proliferate along with MISS during times of stress and use the mats as an ecological niche.

The pectinacean bivalve *Claraia* also proliferated during the deleterious conditions of the Early Triassic (Wignall, 1992; Schubert & Bottjer, 1995). Unlike lingulid brachiopods, this genus of bivalve only existed from the Late Permian to the Middle Triassic. While *Claraia* is now extinct, they are similar to marine flat clams that are morphologically comparable and are typically associated with oxygen-deficient settings (Hallam & Wignall, 1992; Schubert & Bottjer, 1995). In this study, *Claraia* were found consistently associated with MISS, indicating that these bivalves were able to survive the dysoxic to anoxic conditions the microbial mats created.

The relatively small size and simplicity of the trace fossils found are indicative of the recovery and continued environmental stresses in the Early Triassic (Pruss et al., 2004). Horizontal and relatively shallow burrows, like ones created by *Planolites* and *Thalassinoides,* require low-oxygen conditions, as would be present with microbial mats on the surface (Twitchett and Wignall, 1996; Pruss et al., 2004). The smaller size of the

trace-making organisms, due to the Lilliput Effect following the PTME, explain the relatively small size of these traces compared to post recovery (Twitchett, 2007; Algeo et al., 2011).

MISS as an Ecological Niche

To confirm the212 hypothesis that MISS provided an ecological niche for certain metazoans during the Early Triassic, two working hypotheses were developed. These are that MISS proliferated in the subtidal realm during the Early Triassic, and that shelled invertebrates are found in close association with these MISS.

The initial step to supporting these hypotheses was the confirmation of definitive MISS. All of the samples from Hidden Pasture, Montpelier Canyon, and Bear Lake fall under the category of microbially induced phenomena in Pettijohn and Potter's (1964) classification of primary sedimentary structures, which was updated with a new subsection by Noffke in 2001. These determinations were made based on a combination of physical and microscopic characteristics consistent with MISS.

The proliferation of MISS during the Early Triassic can be concluded based on two lines of evidence. First, three of the four localities in this study show the presence of MISS. The actual presence of MISS is likely greatly underrepresented due to a small taphonomic preservation window these fossils have. Additionally, MISS are found consistently in subtidal settings at all three localities, indicating their substantial presence in environmental settings that they only inhabit during periods of ecological

stress. Therefore, the interpretation of this cross section of the western United States seems to confirm the proliferation of MISS in subtidal settings during the Early Triassic.

This study also looked at the geochemical implications for Early Triassic MISS. Recent geochemical evidence suggests localized anoxia and euxinia in an expanded OMZ, with suboxic conditions on Panthalassan bottom waters (Algeo et al., 2008, 2010, 2011). Episodic upwelling of the OMZ would have then brought anoxic, H_2S, and carbon dioxide rich waters onto the shallow continental shelf and platforms. However, the geochemical data collected for the seven samples examined shows that the bottom waters of sediments containing MISS were oxic to suboxic (at most). This would indicate that anoxic bottom waters are not needed for the proliferation of MISS. However, the proliferation of microbial mats would have created anoxic and euxinic porewaters, potentially affecting bottom waters at times and making vertical bioturbation physiologically difficult (McIlroy and Logan, 1999).

Certain disaster taxa, such as lingulid brachiopods and the bivalve *Claraia*, were able to overcome the physical obstacles the microbial mats created and utilize them as an ecological niche. These organisms, along with the trace fossils *Planolites* and *Thalassinoides*, were found consistently associated with MISS in the Lower Triassic strata studied. Morphological evidence has shown that lingulid brachiopods are well adapted to hydrogen sulfide rich environments, while modern analogues of the bivalve *Claraia* show they were well adapted to low oxygen environments (Brunton, 1982; Schubert & Bottjer, 1995; Bailey et al., 2006). Additionally, the trace fossils *Planolites* and *Thalassinoides* are relatively small and simple traces that are indicative of

environmental stresses and require low-oxygen conditions to create (Twitchett & Wignall, 1996; Pruss et al., 2004).

Chapter 11: Conclusion

The evidence for MISS proliferation in the subtidal realm during the Griesbachian, combined with the presence of disaster taxa in close association with these MISS, indicates that MISS likely provided an ecologic niche for certain metazoans during the recovery of the PTME. MISS are found consistently in subtidal settings at all three localities, indicating their substantial presence in subtidal settings even with a strong taphonomic preservational bias. The geochemical data collected suggests that the bottom waters of sediments containing MISS were oxic to suboxic, which is contrary to the general assumption that MISS require anoxic bottom waters to form.

Although the bottom waters were oxic, the microbial mats would have created anoxic and euxinic porewaters, potentially reaching the surface and making vertical bioturbation physiologically difficult. Specific disaster taxa, such as lingulid brachiopods and the bivalve *Claraia*, were able to overcome the physical obstacles the microbial mats created and were found consistently throughout the three localities associated with MISS. The frequency of only a select group of metazoans found in association with bedding planes containing MISS leads to the conclusion that only organisms with specialized adaptations could survive the harsh environments created by the microbial mats. These mats then created an ecological niche for these organisms as they provided a food source in a low competition environment.

REFERENCES

Algeo, T.J., et al. "Association of [34]S-depleted pyrite layers with negative carbonate δ^{13}C excursions at the Permian-Triassic boundary: Evidence for upwelling of sulfidic deep-ocean water masses." *Geochemistry, Geophysics, Geosystems* 9.4 (2008).

Algeo, T. J., et al. "Changes in productivity and redox conditions in the Panthalassic Ocean during the latest Permian." *Geology* 38.2 (2010): 187-190.

Algeo, T. J., et al. "Spatial variation in sediment fluxes, redox conditions, and productivity in the Permian–Triassic Panthalassic Ocean." *Palaeogeography, Palaeoclimatology, Palaeoecology* 308.1 (2011): 65-83.

Algeo, T. J., et al. "Terrestrial–marine teleconnections in the collapse and rebuilding of Early Triassic marine ecosystems." *Palaeogeography, Palaeoclimatology, Palaeoecology* 308.1 (2011): 1-11.

Bailey, J. V., et al. "Microbially-Mediated Environmental Influences on Metazoan Colonization of Matground Ecosystems: Evidence from the Lower Cambrian Harkless Formation." *Palaios* 21.3 (2006): 215-26. Print.

Bender, M.L., and Heggie, D.T. "Fate of organic carbon reaching the deep sea floor: a status report" (1984): Geochimica et Cosmochimica Acta, v. 48, p. 977–986.

Benton, M.J., and R. J. Twitchett. "How to kill (almost) all life: the end-Permian extinction event." *Trends in Ecology & Evolution* 18.7 (2003): 358-365.

Black, B.A., Elkins-Tanton, L.T., and Rowe, M.C. "Magnitude and Consequences of Volatile Release from the Siberian Traps." *Elsevier* (2012): 363-73. Print.

Bottjer, D.J., "Biotic recovery from mass extinctions: *in* Briggs, D., and Crowther, P., eds., Palaeobiology II." (2001): Blackwell Science, Oxford, p. 204–208.

Breithaupt, B. H., Matthews, N. A., & Noble, T. A. (2004). An integrated approach to three- dimensional data collection at dinosaur tracksites in the Rocky Mountain West. *Ichnos*, *11*(1-2), 11-26.

Brennecka, G. A., et al. "Rapid expansion of oceanic anoxia immediately before the end-Permian mass extinction." *Proceedings of the National Academy of Sciences* 108.43 (2011): 17631-17634.

Brunton, C.H., "The functional morphology and palaeoecology of the Dinantian brachiopod Levitusia." *Lethaia* 15.2 (1982): 149-167.

Burgess, S. D., S. Bowring, and S. Shen. "High-precision timeline for Earth's most severe extinction." *Proceedings of the National Academy of Sciences* 111.9 (2014): 3316-3321.

Calvert, S. E., and T. F. Pedersen. "Geochemistry of recent oxic and anoxic marine sediments: implications for the geological record." *Marine geology* 113.1 (1993): 67-88.

Clapham, M.E., et al. "The Double Mass Extinction Revisited: Reassessing the Severity, Selectivity, and Causes of the End-Guadalupian Biotic Crisis (Late Permian)." *Paleobiology* 35.1 (2009)

Corsetti, F.A., et al. "Summary of Early Triassic carbon isotope records." *Comptes Rendus Palevol* 4.6 (2005): 473-486.

Decho, A.W. "Microbial exopolymer secretions in ocean environments: their role(s) in food webs and marine processes." *Oceanogr. Mar. Biol. Annu. Rev* 28 (1990): 73-153.

Droser, M.L., and D.J. Bottjer. "A semiquantitative field classification of ichnofabric: Research method paper." *Journal of Sedimentary Research* 56.4 (1986).

Dupraz, C., et al. "Processes of carbonate precipitation in modern microbial mats." *Earth-Science Reviews* 96.3 (2009): 141-162.

Fischer, A. G. and M. A. Arthur. 1977. Secular variations in the pelagic realm,. *in* Cook, H.E., and Enos, P., eds., Deep Water Carbonate Environments: Society of Economic Paleontologists and Mineralogists Special Publication 25, p. 19–51.

Fraiser, M. L., and D. Bottjer. "Elevated atmospheric CO_2 and the delayed biotic recovery from the end-Permian mass extinction." *Palaeogeography, Palaeoclimatology, Palaeoecology* 252.1 (2007): 164-175.

Fraiser, M., A. Dineen, and P. Sheehan. "Recovery vs. Restructuring: Establishing Ecologic Patterns in Early and Middle Triassic Paleocommunities." *AGU Fall Meeting Abstracts*. Vol. 1. 2013.

Froelich, P.N., et al. "Early oxidation of organic matter in pelagic sediments of the eastern equatorial Atlantic: suboxic diagenesis: Geochimica et Cosmochimica Acta, (1979): v. 43, p. 1075–1090.

Gingras, M. K., et al. "Microbially Induced Sedimentary Structures--A New Category Within the Classification of Primary Sedimentary Structures--Discussion." *Journal of Sedimentary Research* 72.4 (2002): 587-88. Print.

Gingras, M. K., J. MacEachern, and S. Dashtgard. "Process ichnology and the elucidation of physico-chemical stress." *Sedimentary Geology* 237.3 (2011): 115-134.

Gould, S.J., Calloway, C.B., 1980. Clams and Brachiopods — ships that pass into the night. Paleobiology 6, 383–396.

Hallam, A., and Wignall, P.B., "Mass Extinctions and Their Aftermath." (1997): Oxford University Press, Oxford, 320 p.

Hagadorn, J. W., and D. J. Bottjer. "Restriction of a late Neoproterozoic biotope; suspect-microbial structures and trace fossils at the Vendian-Cambrian transition." *Palaios* 14.1 (1999): 73-85

Hofmann, R., et al. "New trace fossil evidence for an early recovery signal in the aftermath of the end-Permian mass extinction." *Palaeogeography, Palaeoclimatology, Palaeoecology* 310.3 (2011): 216-226.

Joachimski, Michael M., et al. "Climate warming in the latest Permian and the Permian–Triassic mass extinction." *Geology* 40.3 (2012): 195-198.

Jørgensen, B.B., and Revsbech, N.P. "Diffusive boundary layers and the oxygen uptake of sediments and detritus." (1985): Limnology and Oceanography, v. 30, p. 111–122.

Jørgensen, B. B., D. C. Nelson, and D. M. Ward. 1992. Grazing and bioturbation in modern microbial mats:. *in* Schopf, J.W., and Klen, C., eds., The Proterozoic Biosphere: A Multidisciplinary Approach: Cambridge University Press, Cambridge, p. 295–297.

Kamo, S. L., et al. "Rapid eruption of Siberian flood-volcanic rocks and evidence for coincidence with the Permian–Triassic boundary and mass extinction at 251 Ma." *Earth and Planetary Science Letters* 214.1 (2003): 75-91.

Kiehl, J. T., and C. A. Shields. "Climate simulation of the latest Permian: Implications for mass extinction." *Geology* 33.9 (2005): 757-760.

Kloss, T. "Interpreting the Paleoenvironmental Context of Marine Shales Deposited During the Cambrian Radiation: Global Insights from Sedimentology, Paleoecology, and Geochemistry." (2012).

Knoll, Andrew H., et al. "Paleophysiology and end-Permian mass extinction."*Earth and Planetary Science Letters* 256.3 (2007): 295-313.

Kump, L. R., A. Pavlov, and M. A. Arthur (2005), Massive release of hydrogen sulfide to the surface ocean and atmosphere during intervals of oceanic anoxia. *Geology*, 33, 397–400

Lehrmann, D. J., Ramezani, J., Bowring, S. A., Martin, M. W., Montgomery, P., Enos, P., Jiayong, W. (2006). Timing of recovery from the end-Permian extinction: Geochronologic and biostratigraphic constraints from south China. *Geology*, *34*(12), 1053-1056.

Luo, G., et al. "Stepwise and large-magnitude negative shift in $\delta^{13}C_{carb}$ preceded the main marine mass extinction of the Permian–Triassic Crisis interval." *Palaeogeography, Palaeoclimatology, Palaeoecology* 299.1 (2011): 70-82.

Manwell, C. "Histological specificity of respiratory pigments—II. Oxygen transfer systems involving hemerythrins in sipunculid worms of different ecologies."*Comparative Biochemistry and Physiology* 1.4 (1960): 277-285.

Mata, S. A., and D. J. Bottjer. "Microbes and mass extinctions: paleoenvironmental distribution of microbialites during times of biotic crisis." *Geobiology* 10.1 (2012): 3-24.

Matthews, N. A., & Breithaupt, B. H. (2001). Close-range photogrammetric experiments at Dinosaur Ridge. *The Mountain Geologist*.

McHenry, L. J. "Element mobility during zeolitic and argillic alteration of volcanic ash in a closed-basin lacustrine environment: Case study Olduvai Gorge, Tanzania." *Chemical Geology* 265.3 (2009): 540-552.

McIlroy, D., and G. Logan. "The impact of bioturbation on infaunal ecology and evolution during the Proterozoic-Cambrian transition." *Palaios* 14.1 (1999): 58-72.

Meyer, K. M., L. R. Kump, and A. Ridgwell. "Biogeochemical controls on photic-zone euxinia during the end-Permian mass extinction." *Geology* 36.9 (2008): 747-750.

Nielsen, J. K., and Y. Shen. "Evidence for sulfidic deep water during the Late Permian in the East Greenland Basin." *Geology* 32.12 (2004): 1037-1040.

Noffke, N., Gerdes, G., Klenke, T., & Krumbein, W. E. (2001). Microbially Induced Sedimentary Structures--A New Category within the Classification of Primary Sedimentary Structures: PERSPECTIVES. *Journal of Sedimentary Research*, *71*(5), 649-656.

Noffke, N. "Microbially Induced Sedimentary Structures (MISS) and the Survivor Species Concept." *GSA Annual Convention, Denver Annual Meeting* (2004): n. pag. Print.

Noffke, N. (2009). The criteria for the biogeneicity of microbially induced sedimentary structures (MISS) in Archean and younger, sandy deposits. *Earth-Science Reviews*, *96*(3), 173-180.

"Paleogeography Library," *Global Paleogeography.* Web. <http://cpgeosystems.com/globaltext2.html>.

Paull, R. A., Paull, R. K., 1983. Revision of type Lower Triassic Dinwoody Formation, Wyoming, and designation of principal reference section. Contributions to Geology. v. 22

Paull, R.A., Paull, R.K., "Depositional History of Lower Triassic Rocks in Southwestern Montana and Adjacent Parts of Wyoming and Idaho." *AAPG Bulletin* 73 (1989): n. pag. Print.

Paull, R., and R. Paull. "Shallow Marine Sedimentary Facies in the Earliest Triassic (Griesbachian) Cordilleran Miogeocline, U.S.A." *Sedimentary Geology* 93.3-4 (1994): 181-91. Print.

Payne, J. L., et al. "Large perturbations of the carbon cycle during recovery from the end-Permian extinction." *Science* 305.5683 (2004): 506-509.

Payne, Jonathan L., and Lee R. Kump. "Evidence for recurrent Early Triassic massive volcanism from quantitative interpretation of carbon isotope fluctuations." *Earth and Planetary Science Letters* 256.1 (2007): 264-277.

Pettijohn, F.J., AND Potter, P.E., "Atlas and Glossary of Primary Sedimentary Structures." (1964): Berlin, Springer-Verlag, 370 p

Pierson, B.K., et al. "Modern mat-building microbial communities: a key to the interpretation of Proterozoic stromatolitic communities." (1992) In: Schopf, J.W., Klein, C. (Eds.), The Proterozoic Biosphere. Cambridge University Press, New York, pp. 241–242.

Pruss, S., Fraiser, M., and Bottjer, D., "Proliferation of Early Triassic Wrinkle Structures: Implications for Environmental Stress following the End-Permian Mass Extinction." *Geology* 32.5 (2004): 461. Print.

Pruss, Sara B., and David J. Bottjer. "Early Triassic trace fossils of the western United States and their implications for prolonged environmental stress from the end-Permian mass extinction." *Palaios* 19.6 (2004): 551-564.

Pruss, S. B., Corsetti, F. A., & Bottjer, D. J. (2005). The unusual sedimentary rock record of the Early Triassic: A case study from the southwestern United States. *Palaeogeography, Palaeoclimatology, Palaeoecology*, *222*(1), 33-52.

Rampino, Michael R., and Ken Caldeira. "Major perturbation of ocean chemistry and a 'Strangelove Ocean'after the end-Permian mass extinction." *Terra Nova* 17.6 (2005): 554-559.

Raup, David M. "Size of the Permo-Triassic bottleneck and its evolutionary implications." *Science* 206.4415 (1979): 217-218.

Reichow, M., M. Pringle, A. Almukhamedov, M. Allen, V. Andreichev, M. Buslov, C. Davies, G. Fedoseev, J. Fitton, and S. Inger. "The Timing and Extent of the Eruption of the Siberian Traps Large Igneous Province: Implications for the End-Permian Environmental Crisis." *Earth and Planetary Science Letters* 277.1-2 (2009): 9-20. Print.

Reimers, C.E., and Suess, E. "Spatial and temporal patterns of organic matter accumulation on the Peru continental margin." (1983): *in* Thiede, J., and Suess, E., eds., Coastal Upwelling: Its Sediment Record, Part B. Sedimentary Records of Ancient Coastal Upwelling: Plenum Press, New York, p. 311–346.

Retallack, G. J., and A.H. Jahren. "Methane release from igneous intrusion of coal during Late Permian extinction events." *The Journal of Geology* 116.1 (2008): 1-20.

Retallack, G. J. "Postapocalyptic greenhouse paleoclimate revealed by earliest Triassic paleosols in the Sydney Basin, Australia." *Geological Society of America Bulletin* 111.1 (1999): 52-70.

Riccardi, Anthony, et al. "Carbon isotopic evidence for chemocline upward excursions during the end-Permian event." *Palaeogeography, Palaeoclimatology, Palaeoecology* 248.1 (2007): 73-81.

Rodland, D. L. (1999). Paleoenvironments and paleoecology of the disaster taxon Lingula in the aftermath of the end-Permian mass extinction: Evidence from the Dinwoody Formation (Griesbachian) of southwestern Montana and western Wyoming: Unpulished MS Thesis. *University of Southern California, Los Angeles*.

Rodland, David L., and David J. Bottjer. "Biotic recovery from the end-Permian mass extinction: behavior of the inarticulate brachiopod Lingula as a disaster taxon." *Palaios* 16.1 (2001): 95-101.

Schaefer, S. (2012). Distribution of Early Triassic Rhynchonelliform Brachiopods in the Dinwoody Basin of the Western United States: A Test of the Habitable Zone Hypothesis (Master's Thesis, University of Wisconsin--Milwaukee).

Schieber, Juergen. "Microbial mats in terrigenous clastics; the challenge of identification in the rock record." *Palaios* 14.1 (1999): 3-12.

Schieber, J., P. K. Bose, P. G. Eriksson, S. Banerjee, S. Sarkar, W. Altermann, and O. Catuneanu. *Atlas of Microbial Mat Features Preserved Within the Siliciclastic Rock Record*. Amsterdam: Elsevier, 2007. Print.

Schock, W. W. (1981). *Stratigraphy and paleontology of the Lower Dinwoody Formation and its relation to the Permian-Triassic boundary in western Wyoming, southeastern Idaho and southwestern Montana* (Doctoral dissertation, University of Wyoming).

Schubert, J.K., and Bottjer, D.J. "Aftermath of the Permian-Triassic Mass Extinction Event: Paleoecology of Lower Triassic Carbonates in the Western USA." *Palaeogeography, Palaeoclimatology, Palaeoecology* 116.1-2 (1995): 1-39. Print.

Sepkoski, J.J., 1981. A factor analytic description of the Phanerozoic marine fossil record. Paleobiology 7 (1), 36–53.

Shen, J., et al. "Volcanic perturbations of the marine environment in South China preceding the latest Permian mass extinction and their biotic effects."*Geobiology* 10.1 (2012): 82-103.

Shen, Shu-Zhong, et al. "Biostratigraphy and lithofacies of the Permian System in the Laibin–Heshan area of Guangxi, South China." *Palaeoworld* 16.1 (2007): 120-139.

Sun, Y., et al. "Lethally hot temperatures during the Early Triassic greenhouse." *Science* 338.6105 (2012): 366-370.

Takahashi, S., et al. "Bioessential element-depleted ocean following the euxinic maximum of the end-Permian mass extinction." *Earth and Planetary Science Letters* 393 (2014): 94-104.

"The Basics of Photogrammetry." *Geodetic Systems, Inc.* N.p., n.d. Web. http://www.geodetic.com/v-stars/what-is-photogrammetry.aspx

Tribovillard, N., et al. "Trace metals as paleoredox and paleoproductivity proxies: an update." *Chemical Geology* 232.1 (2006): 12-32.

Twitchett, R.J. "The Lilliput effect in the aftermath of the end-Permian extinction event." *Palaeogeography, Palaeoclimatology, Palaeoecology* 252.1 (2007): 132-144.

Twitchett, R. J., and P.B. Wignall. "Trace fossils and the aftermath of the Permo-Triassic mass extinction: evidence from northern Italy." *Palaeogeography, Palaeoclimatology, Palaeoecology* 124.1 (1996): 137-151.

Wedepohl, K. H. "Environmental influences on the chemical composition of shales and clays." *Physics and Chemistry of the Earth* 8 (1971): 305-333.

Wignall, P. B., and A. Hallam. "Anoxia as a cause of the Permian/Triassic mass extinction: facies evidence from northern Italy and the western United States." *Palaeogeography, Palaeoclimatology, Palaeoecology* 93.1 (1992): 21-46.

Wignall, P. B., and A. Hallam. "Griesbachian (Earliest Triassic) palaeoenvironmental changes in the Salt Range, Pakistan and southeast China and their bearing on the Permo-Triassic mass extinction." *Palaeogeography, Palaeoclimatology, Palaeoecology* 102.3 (1993): 215-237.

Xie, Shucheng, et al. "Changes in the global carbon cycle occurred as two episodes during the Permian–Triassic crisis." *Geology* 35.12 (2007): 1083-1086.

Yan, Zheng, et al. "Features of stable isotope near the Permian-Triassic boundary of the Shangsi section, Guangyuan, Sichuan." Study on the Permian–Triassic biostratigraphy and event stratigraphy of northern Sichuan and Southern Shaanxi: Beijing, Geological Publishing House (1989): 166-171.

Zhang, Z., and Han, J. "Soft–tissue Preservation in the Lower Cambrian Linguloid Brachiopod from South China." *Acta Palaeontol. Pol.* 49 (2004): n. pag. Print.